Check for updates

AGU ADVANCING EARTH AND SPACE SCIENCES

Water Resources Research

RESEARCH ARTICLE
10.1029/2024WR038860

Model Inputs and Data Requirements for Process-Based Stream Temperature Modeling in Regulated Peri-Alpine Rivers

David Dorthe[1,2], **Michael Pfister**[1], **and Stuart N. Lane**[2]

[1]School of Engineering and Architecture of Fribourg, HES-SO University of Applied Sciences and Arts Western Switzerland, Fribourg, Switzerland, [2]Faculty of Geosciences and Environment, Institute of Earth Surface Dynamics, University of Lausanne, Lausanne, Switzerland

Key Points:

- A stream temperature process-based model was calibrated for a regulated river based on an extensive stream temperature data set
- Correction of solar radiation for local shading and heat fluxes with the sediment layer were found to be crucial
- High accuracy across space and time was achieved with few parameters, enabling practical use in river management

Supporting Information:

Supporting Information may be found in the online version of this article.

Correspondence to:

D. Dorthe,
david.dorthe@hefr.ch

Citation:

Dorthe, D., Pfister, M., & Lane, S. N. (2025). Model inputs and data requirements for process-based stream temperature modeling in regulated Peri-Alpine rivers. *Water Resources Research*, *61*, e2024WR038860. https://doi.org/10.1029/2024WR038860

Received 6 SEP 2024
Accepted 26 JUL 2025

© 2025. The Author(s).
This is an open access article under the terms of the Creative Commons Attribution-NonCommercial-NoDerivs License, which permits use and distribution in any medium, provided the original work is properly cited, the use is non-commercial and no modifications or adaptations are made.

Abstract Regulated rivers can experience sharp temperature variations induced by intermittent hydropower production (thermopeaking). To mitigate ecological impacts, dam operators need to assess the impacts of hydropeaking on stream temperature, and to test scenarios that might reduce them. While stream temperature modeling has been investigated in numerous studies, few have systematically assessed how integrated processes and their representation affect model performance, and models capable of capturing both sub-hourly variations and long-term thermal dynamics remain a challenge. Herein, a stream temperature model within the HEC-RAS platform was used to model the thermal regime of a regulated river in Switzerland, with a 10-min timestep over the annual time-scale and for a 22-km long reach; and for which we had installed a network of stream temperature sensors. While the initial model demonstrated an acceptable performance at the yearly scale (Mean Absolute Error: 0.78–2.10°C and Kling-Gupta Efficiency: 0.55–0.85), this was not the case at the daily or seasonal time-scales. Two model corrections were found to be crucial; (a) the correction of potential incoming solar radiation for local shading; and (b) the representation of the heat flux linked to water-sediment exchanges. With these two corrections, the annual performance improved (*MAE*: 0.48–0.83°C and *KGE*: 0.85–0.93) as did the daily and seasonal performance. Although physically based, the model required calibration, underscoring the importance of high-quality in situ temperature data. The resulting model proves effective for practical applications in hydropower mitigation and river temperature management under complex flow regimes.

1. Introduction

Stream temperature plays a critical role in shaping aquatic habitats and regulating ecological processes, and its importance is expected to grow as climate change raises river temperatures (Ouellet et al., 2020; van Vliet et al., 2013; Wanders et al., 2019). It is of particular concern for the management of regulated rivers where intermittent hydropower production can cause abrupt stream temperature variations, known as thermopeaking (Zolezzi et al., 2011) that may harm aquatic ecosystems (Auer et al., 2023; Mameri et al., 2023). These challenges call for targeted responses, which in turn require robust models to predict thermal dynamics and evaluate management scenarios. This study focuses on the influence of model structure and parameterization on the performance of a process-based model, for regulated rivers affected by thermopeaking.

Statistical and process-based mathematical models simulating river temperatures have been developed with some success in recent decades. Statistical models estimate stream temperature by establishing empirical relationships with environmental variables (Caissie, El-Jabi, & Turkkan, 2014; Leach et al., 2023). Recent advances in machine learning and deep learning have improved predictive accuracy (Rahmani et al., 2021; Zhu & Piotrowski, 2020), but these approaches require substantially more data than simpler models (O'Sullivan et al., 2020; Toffolon & Piccolroaz, 2015). Their main limitation is that they are valid only within the range of conditions represented in the training data (Benyahya et al., 2007; Topp et al., 2023), making them unsuitable for predicting stream temperature under changing conditions. Although they are sometimes used to project stream temperature under climate change scenarios (e.g., Sun et al., 2024) the reliability of such extrapolations remains limited and should be interpreted with caution. Process-based models address this limitation by quantifying heat fluxes through a physical representation (Dugdale et al., 2017), enabling the assessment of stream temperature responses to modifications. Such models have recently been used to evaluate the effects of restoration strategies on thermal river regimes (Abdi et al., 2021; Dugdale et al., 2024; Hall & Selker, 2021). These models require extensive

19447973, 2025, 9, Downloaded from https://agupubs.onlinelibrary.wiley.com/doi/10.1029/2024WR038860 by Schweizerische Akademie Der, Wiley Online Library on [26/09/2025]. See the Terms and Conditions (https://onlinelibrary.wiley.com/terms-and-conditions) on Wiley Online Library for rules of use; OA articles are governed by the applicable Creative Commons License

boundary and calibration data to estimate heat fluxes accurately at the air–water and streambed interfaces (Dugdale et al., 2017).

Air-water heat fluxes at the water surface have been identified as the main processes driving stream temperature (Caissie et al., 2005; Sinokrot & Stefan, 1993). Solar radiation and, by extension, riparian shading are thought to exert the greatest influence. Research has shown that shading, whether due to vegetation or relief, has an important impact on stream temperatures (Garner et al., 2017; Hannah et al., 2008; Leach & Moore, 2010; Malcolm et al., 2004) and needs to be incorporated into associated models (Dugdale et al., 2017; St-Hilaire et al., 2000). Although the need to account for shading effects is well recognized, the methods used to define and incorporate this factor varies (Dugdale et al., 2024; Maheu & Caissie, 2023; Trimmel et al., 2018; Wawrzyniak et al., 2017).

Heat exchanges occurring at the streambed interface were further identified as important process in the river heat budget (Hannah et al., 2004; Leach & Moore, 2014; Poole & Berman, 2001; Webb & Zhang, 1997) and applied to stream temperature modeling (Birkel et al., 2016; Caissie, Kurylyk, et al., 2014; Moore et al., 2005; Sinokrot & Stefan, 1993). Streambed exchanges are typically a combination of several processes such as bed conduction, hyporheic exchange and bed friction (Leach et al., 2023) that can be individually quantified (Caissie & Luce, 2017), but are usually aggregated since they are difficult to partition in modeling approaches (Hannah et al., 2004). The influence of hyporheic processes is thought to be negligible for the surface temperature in unregulated rivers (Hester et al., 2009), but will be increased with artificial daily water level fluctuations (Boutt & Fleming, 2009; Sawyer et al., 2009). These fluxes are difficult to quantify because data on sediment layer properties are often incomplete and heterogeneous (Birkel et al., 2016; Trimmel et al., 2018). However, calibration approaches targeting either sediment characteristics (Dugdale et al., 2024) or the resulting heat flux (Wade et al., 2024) have been applied.

Although process-based stream temperature models are now widely available, there is no clear guidance as to which processes should be included, and how they should be represented to simulate the thermal regime of regulated rivers accurately. As the number and complexity of processes increase, so does the number of parameters and data requirements, highlighting the need for model parsimony (Beven, 2018). To address this trade-off, model complexity should be informed by its predictive performance for a given purpose (Hrachowitz et al., 2014). Assessing performance requires high-quality data and carefully selected evaluation criteria. Since commonly used statistical metrics may be insufficient, purpose-oriented indicators specific to the intended model application should also be considered (Beven & Lane, 2022; Ritter & Muñoz-Carpena, 2013; Todorović et al., 2022).

Modeling stream temperature in regulated rivers subjected to thermopeaking presents a distinctive challenge. Given the typical occurrence of turbine switch on/off events within a 15–60 min window, capturing these rapid temperature changes requires models with sub-hourly resolution (Vanzo et al., 2016), along with input and calibration data of equally high temporal detail (Zolezzi et al., 2011). While stream temperature modeling has previously been applied to regulated systems, these studies have often focused on daily resolution, limiting their ability to capture short-term thermal dynamics (Beaupré et al., 2020; Cole et al., 2014).

Models that capture the spatio-temporal variations and signatures in stream temperature, particularly under regulated regimes, could help to predict future thermal regimes under scenarios such as climate change and hydropeaking mitigation. Despite growing interest in this topic, few studies have focused on the short-term variability induced by thermopeaking. Moreover, most rely on sparse data sets, limiting the ability to assess systematically how model performance evolves under different parameterization choices. Existing studies that do investigate parameterization effects have generally focused on short summer periods, in unregulated rivers, and at only one or two cross-sections (Wade et al., 2024; Wawrzyniak et al., 2017).

To address these gaps, this study is based on a high temporal-resolution, multi-year, multi-site stream temperature data set. Its main objective is to analyse how the performance of a process-based model evolves depending on the thermal processes integrated. The study also examines the data requirements and performance indicators needed to evaluate model quality. More broadly, it contributes to the ongoing discussion on balancing model complexity and data availability to develop models that are both purpose-driven and practice-oriented.

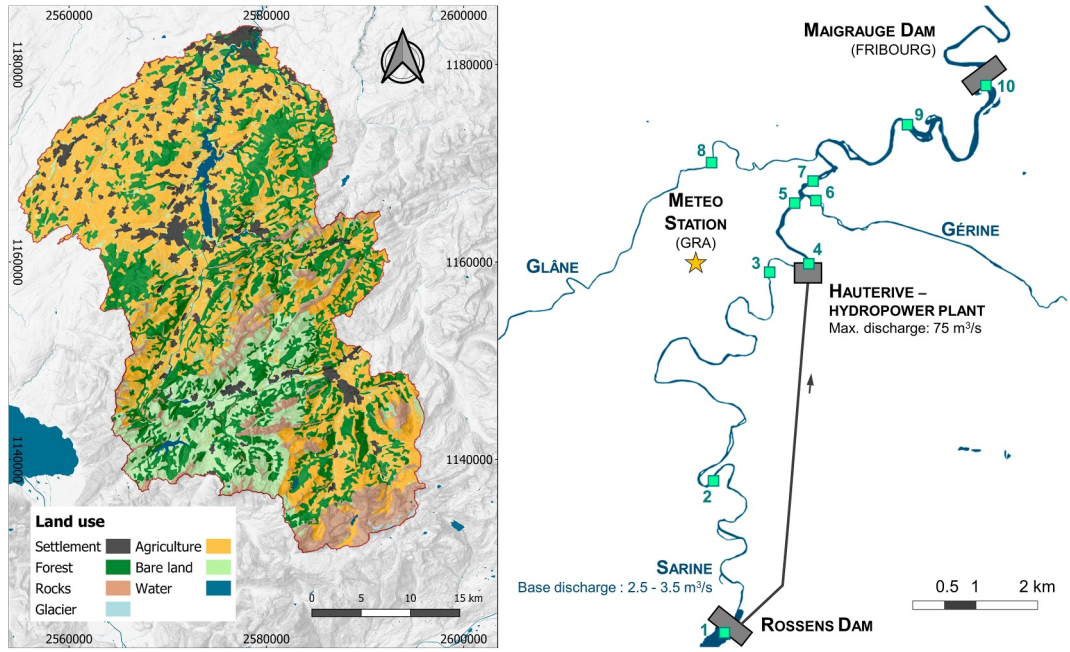

Figure 1. Watershed of the study reach of the Sarine with land use information (left) and study reach of the Sarine with main hydraulic structures and location of measuring stations along the reach (right) (background: © swisstopo data).

2. Data and Methods

2.1. Study Site

The Sarine is a regulated river flowing from the Swiss Alps to the Aare, a tributary of the Rhine. Extending for 126 km it drains a catchment of 1,892 km^2 with elevations ranging from 2,540 m asl in the Alps to 461 m asl at the confluence with the Aare River. Along its course, five dams regulate the river and supply water to hydropower plants. The study site is a 22 km reach of the Sarine located between two dams: the Rossens dam upstream which forms Lake Gruyère and the Maigrauge dam downstream which forms Lake Pérolles. The altitude in this reach ranges from 608 m at the base of the Rossens dam to 553 m in the Lake Pérolles.

By the end of the studied reach (city of Fribourg), the watershed considered covers 1,269 km^2 with a mean annual discharge of 41.6 m^3/s. The Sarine is joined by two main tributaries, the Gérine and the Glâne, both unregulated, with a mean annual discharge of respectively 1.7 and 4.2 m^3/s. The minimum residual flow released into the Sarine downstream of Lake Gruyère is 3.5 m^3/s from May to September and 2.5 m^3/s for the rest of the year. The Hauterive hydropower plant located at 13.5 km downstream of Lake Gruyère turbines and releases water drawn from the lake after its conveyance through a 6 km long gallery (Figure 1). The maximum flow that can be turbined at the hydropower plant is 75 m^3/s thus inducing strong variations of the river regime linked to hydropeaking.

While the Sarine is predominantly a gravel-bed river, sediment transport is modified strongly by the presence of lakes and dams. In some sections, sediment scarcity has resulted in complete erosion of the sediment layer, exposing bedrock. Lack of sediment is compensated by occasional artificial sediment addition and artificial floods, and naturally through sediment supply from tributaries, mainly the Gérine.

The closest meteorologic station at Fribourg/Grangeneuve (MeteoSwiss) shows an average annual air temperature of 9.1°C that ranges between mean monthly values of 0.4°C in January and 18.5°C in July (period 1991–2020). The mean yearly precipitation between 1991 and 2020 was 962 mm.

Lake Gruyère exhibits rapid surface temperature variations driven by atmospheric conditions. A much weaker annual temperature cycle occurs below the thermocline. At the level of the gallery intake, 40 m below the maximum lake level, water temperature typically ranges between a minimum of 3°C in February and a maximum of 15°C in September (data from hydropower operator).

19447973, 2025, 9, Downloaded from https://agupubs.onlinelibrary.wiley.com/doi/10.1029/2024WR038860 by Schweizerische Akademie Der, Wiley Online Library on [26/09/2025]. See the Terms and Conditions (https://onlinelibrary.wiley.com/terms-and-conditions) on Wiley Online Library for rules of use; OA articles are governed by the applicable Creative Commons License

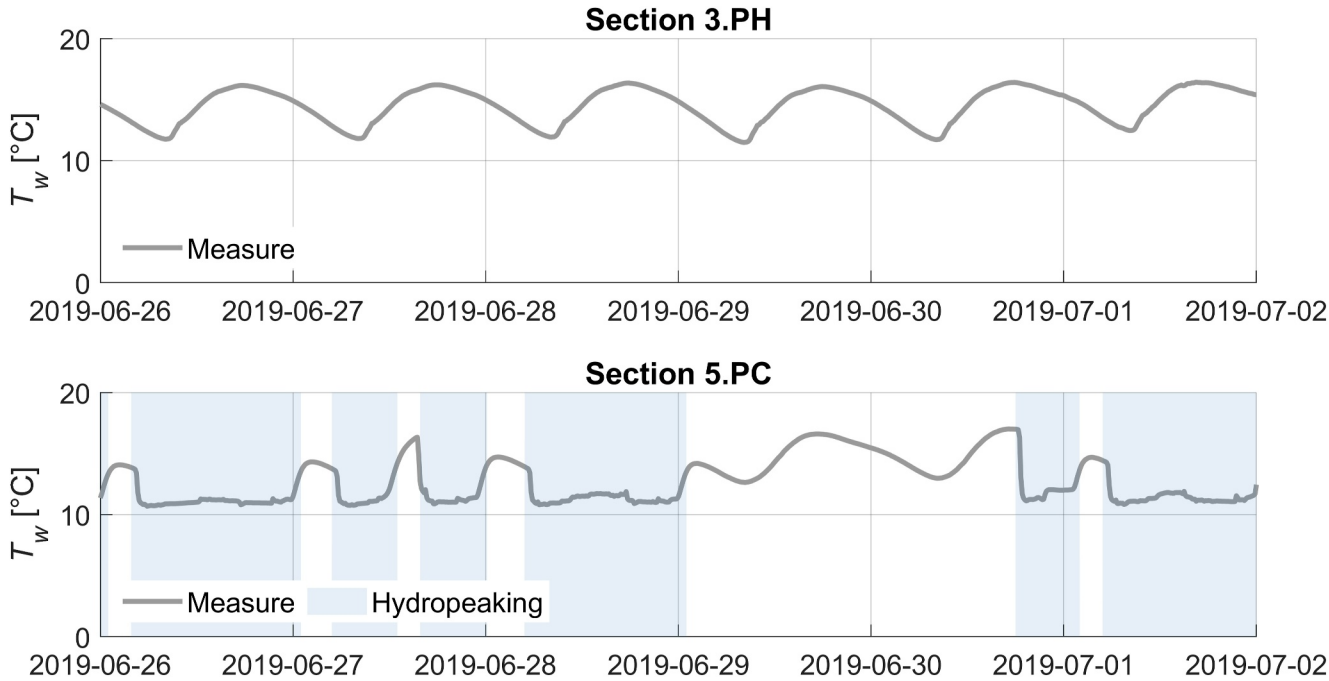

Figure 2. Example of stream temperature measurements at two different sections for a 10-day period in summer 2019 (sections from Figure 1).

In the 6 km bedrock gallery between the dam and the power plant, the conveyed flow undergoes minimal temperature variations. In contrast, the river flowing in parallel experiences temperature fluctuations due to natural atmospheric and environmental conditions, and then downstream of the power plant due to hydropeaking (Figure 2).

2.2. Numerical Model

In this study, HEC-RAS 1D (HEC, 2022) was used because in representing unsteady hydrodynamics at a fine temporal resolution it is well suited to capturing the short-term thermal effects of thermopeaking in a river that is largely single thread throughout its length. A 1D approach was preferred over higher-dimensional models, as it enables simulation over the 22 km study reach while keeping data and computational requirements manageable. However, it does not resolve within-section thermal heterogeneity, which may be important near release points where mixing is incomplete.

HEC-RAS integrates a water quality module that simulates fate and transport of water temperature coupled to a steady or unsteady treatment of 1D hydrodynamics. The model is divided into "water quality cells" in which a single value of water temperature is defined. These cells can be defined by two successive hydraulic sections or combined into larger cells. Water temperature is calculated using a heat budget for each cell either acting as a heat "source" or "sink" according to whether heat energy is increased or decreased (Brunner, 2016). The heat budget is given as:

$$\text{Heat}_{\text{Source/Sink}} = \frac{q_{\text{net}}}{\rho_w c_{pw}} \frac{A_s}{V} \tag{1}$$

where q_{net} is the net heat flux (W m^{-2}), ρ_w the density of water (kg m^{-3}), c_{pw} the specific heat of water at constant pressure (J kg^{-1} °C^{-1}), A_s and V the area (m^2) and volume (m^3) of a water quality cell.

The net heat flux is expressed as:

$$q_{\text{net}} = q_{sw} + q_{\text{atm}} - q_b + q_h - q_l + q_{\text{sed}} \tag{2}$$

19447973, 2025, 9, Downloaded from https://agupubs.onlinelibrary.wiley.com/doi/10.1029/2024WR038860 by Schweizerische Akademie Der, Wiley Online Library on [26/09/2025]. See the Terms and Conditions (https://onlinelibrary.wiley.com/terms-and-conditions) on Wiley Online Library for rules of use; OA articles are governed by the applicable Creative Commons License

19447973, 2025, 9, Downloaded from https://agupubs.onlinelibrary.wiley.com/doi/10.1029/2024WR038860 by Schweizerische Akademie Der, Wiley Online Library on [26/09/2025]. See the Terms and Conditions (https://onlinelibrary.wiley.com/terms-and-conditions) on Wiley Online Library for rules of use; OA articles are governed by the applicable Creative Commons License

where q_{sw} is the solar radiation (W m^{-2}), q_{atm} the atmospheric (downwelling) longwave radiation (W m^{-2}), q_b the back (upwelling) longwave radiation, q_h the sensible heat (W m^{-2}), q_l the latent heat (W m^{-2}), q_{sed} the sediment-water heat flux (W m^{-2}).

These terms are derived from time-varying atmospheric data and from local stream characteristics such as bathymetry and roughness, which are assumed to remain constant over time. This could limit the model's ability to simulate stream temperature in a multi-year context, as potential changes in channel characteristics are not accounted for. The temperature model allows for the use of measured solar radiation values but does not include any algorithm to account for shading effects. To account for this limitation, solar radiation must be pre-processed externally to correct the input data accordingly (see Section 2.4). The model does not account for ice formation, but this process is negligible along the studied reach.

The sediment heat flux of Zhang and Johnson (2016) simulates heat exchange within bed sediment from the sediment-water interface to user-defined depth. Incorporating such a process is important in a hydropower-impacted river because water retention in dams may lead to long periods with a minimum flow with shallow flow depths, warmer temperatures and hence heat flux into the bed. This may reverse during winter periods. In the Zhang and Johnson (2016) treatment, temperature variation is driven by exchange with the water column, based on:

$$\rho_s C_{ps} \frac{dT_{\text{sed}}}{dt} = -\frac{q_{\text{sed}}}{h_2} \tag{3}$$

where ρ_s is the density of the sediment layer (kg m^{-3}), C_{ps} the specific heat capacity of the sediment layer (J kg^{-1} °C^{-1}), T_{sed} the sediment layer temperature, q_{sed} the sediment-water heat flux (W m^{-1}) and h_2 the active sediment layer thickness (m). The sediment–water heat flux (q_{sed}) is expressed as:

$$q_{\text{sed}} = \rho_s C_{ps} \frac{\alpha_s}{0.5 h_2} (T_{\text{sed}} - T_w) \tag{4}$$

where α_s is the sediment thermal diffusivity (m^2 s^{-1}).

This heat flux accounts only for conduction and diffusion, without considering convective heat fluxes. It also assumes spatially homogeneous and temporally constant sediment properties, which may limit the accuracy of simulated streambed temperature dynamics under varying flow or thermal conditions. A temperature boundary condition for the bottom of the sediment layer is required. The sediment layer acts as a composite element situated at the interface between the water and the deeper layers of the ground. While the water column exhibits significant sub-daily fluctuations and the ground temperature remains almost constant (Brunke & Gonser, 1997), it was assumed that the sediment layer boundary condition will undergo temperature variations over an annual cycle. This boundary condition was computed by using a weighted average based on both the mean groundwater temperature at the study site and a moving average of the air temperature from preceding days to account for seasonal variability. The time-dependant boundary condition $T_{\text{sed}}(t)$ was expressed as:

$$T_{\text{sed}}(t) = w_1 \cdot \overline{T}_{gw} + w_2 \cdot \overline{T}_{\text{air}[t-\Delta t;t]} \tag{5}$$

with w_1 and w_2 the respective ponderation for both terms, $\overline{T}_{gw}$ the long-term mean groundwater temperature and $\overline{T}_{\text{air}[t-\Delta t;t]}$ the moving average of air temperature for the last Δt days before the time t (Text S1 in Supporting Information S1).

Given the challenges of directly measuring sediment layer properties (Birkel et al., 2016; Trimmel et al., 2018), a multi-parameter calibration approach was applied using our extensive water temperature data set to estimate appropriate sediment properties and boundary condition coefficients (see Section 2.6).

2.3. Data Collection

Our simulations used input data representing the main drivers of heat exchange processes, including discharge, bathymetry, meteorological conditions, and the temperature of water inflows at the model boundaries. Stream

19447973, 2025, 9, Downloaded from https://agupubs.onlinelibrary.wiley.com/doi/10.1029/2024WR038860 by Schweizerische Akademie Der, Wiley Online Library on [26/09/2025]. See the Terms and Conditions (https://onlinelibrary.wiley.com/terms-and-conditions) on Wiley Online Library for rules of use; OA articles are governed by the applicable Creative Commons License

Table 1
List of Collected Data With Section, Time Resolution and Source

Section	ID	Collected data	Temporal resolution	Source
1. Rossens	RO	Lake temperature profile Released discharge	6-hr (constant)	HP operator HP operator
2. Châteaux	CH	Stream temperature	10-min	Dorthe et al. (2025)
3. Passerelle Hauterive	PH	Stream temperature	10-min	Dorthe et al. (2025)
4. Hydropower Plant	HP	Stream temperature Released discharge	10-min 1-hr	Dorthe et al. (2025) HP operator
5. Passerelle Confluence	PC	Stream temperature	10-min	Dorthe et al. (2025)
6. Gérine	GE	Stream temperature Tributary discharge	10-min 1-hr	Dorthe et al. (2025) Swissriver (2025)
7. Interconfluence	IC	Stream temperature	10-min	Dorthe et al. (2025)
8. Glâne	GL	Stream temperature Tributary discharge	10-min 1-hr	Dorthe et al. (2025) Swissrivers (2025)
9. Rittes	RI	Stream temperature	10-min	Dorthe et al. (2025)
10. Maigrauge	MA	Stream temperature	10-min	Dorthe et al. (2025)
Meteorological Station		Air temperature Solar radiation Atm. Pressure Wind velocity Air humidity	10-min 10-min 10-min 10-min 10-min	MeteoSwiss (2025)

water temperature measurements were also used to compare model outputs and support calibration and validation. The data, collected between 2017 and 2024, are listed in Table 1.

2.3.1. Driving Factors

The base discharge released at Rossens dam (constant at 2.5 m^3/s except from May to September with 3.5 m^3/s) and the discharge conveyed through the power plant were provided by the hydropower operator over the entire monitoring period. Discharge measurements for the two main tributaries were obtained near the confluence, with time-series data downloaded from fribourg.swissrivers.ch (Swissrivers, 2025). Bathymetric data comprising 108 section profiles along the 22 km river reach and measured in 2014 were provided by the Federal Office for the Environment (FOEN), with a maximal spacing of 250 m between successive sections. A comparison with previous section measurements carried out in 2000 and 2006 showed that morphological evolutions are limited on this reach.

The meteorological data required to compute the model heat fluxes were sourced from a Federal Office of Meteorology and Climatology (MeteoSwiss, 2025) station located centrally in the study area (Fribourg/Grangeneuve, GRA, Figure 1). MeteoSwiss data were collected through an automatic monitoring network, with systematic quality control procedures applied to ensure completeness and plausibility. The following data were used, with a 10 min resolution: air temperature, solar radiation, atmospheric pressure, wind velocity and air humidity.

Water temperatures are measured in Gruyère Lake, at the Rossens dam by the operator. These measurements, taken at four different depths, enable the estimation of the temperature of the base discharge released at the toe of the dam and the water captured at the intake, conveyed through the gallery, and released at the hydropower plant. Temperature measurements in the restitution channel of the hydropower plant indicated only minimal temperature differences between the gallery intake and the plant release. The stream temperatures of both tributaries were measured as close as possible to their confluence with the main river course.

2.3.2. Stream Water Temperature

To calibrate and to validate the model, we used high frequency resolution monitoring of stream temperature (10 min interval) for 7 years and at seven monitoring sites, three located upstream of the powerplant and four

19447973, 2025, 9, Downloaded from https://agupubs.onlinelibrary.wiley.com/doi/10.1029/2024WR038860 by Schweizerische Akademie Der, Wiley Online Library on [26/09/2025]. See the Terms and Conditions (https://onlinelibrary.wiley.com/terms-and-conditions) on Wiley Online Library for rules of use; OA articles are governed by the applicable Creative Commons License

downstream (Figure 1). VEMCO Minilog-II-T and HOBO U22-001 temperature loggers were used, characterized by an effective precision of ±0.1°C and ±0.21°C, respectively.

During calibration and validation, measured temperatures were compared to model outputs, which assume uniform temperature distribution within each section. Probes were therefore placed in well-mixed, single-thread channels to ensure they reflected representative average values. Significant fluctuations in water level or external intervention resulted in periods when the probes were not submerged, then recording air temperature instead of stream temperature. To detect these events, thermometers were paired with a HOBO U20L-01 pressure probe. This coupling allowed for the determination of the device's depth in the water column with an effective accuracy of ±0.01 (m) water column. During data pre-processing, pressure measures resulting in a water elevation smaller than the probe's length (0.15 m) were filtered out.

The calibration and validation are mainly carried out with the data from four sections, two located upstream of the power plant (Sections 2.CH and 3.PH) and two located downstream (Sections 5.PC and 9.RI). These four sections have a similar environment, characterized with a gorge topography and a continuous riparian vegetation but are exposed differently to boundary conditions that influence the hydrological and thermal regimes of the river locally. Section 2.CH is located 4 km downstream of the Rossens dam and is thus still strongly influenced by lake temperature. Section 3.PH, is located 12.5 km downstream of Rossens dam and less than 1 km upstream of the power plant. It is the last section that is not influenced by the power plant. Section 5.PC is 1.5 km downstream of the power plant. The water at this section is well-mixed and it is also the last section that is not influenced by the two main tributaries. Finally, Section 9.RI is located 3.5 km downstream of the power plant and 1 km downstream of the confluence with the second tributary. After that, the river starts to be gradually influenced by the presence of the Maigrauge Dam located downstream.

2.4. Solar Shading Correction

The effects of shading at the water surface were computed based on sun position (day, time, latitude) and a digital surface model. Herein, the GRASS-GIS *r.sun* tool (Hofierka & Suri, 2002) was used. The methodology is illustrated in Figure 4. For a given hour and day, the model uses the digital surface model to determine shading and incoming solar radiation at each point. The results are extracted over the river surface area to compute an average incoming radiation. This average is then compared to the theoretical maximum radiation for that specific hour, date, and latitude; the resulting ratio yields a correction factor representing the proportion of global radiation reaching the water surface (Figure 4a). This calculation was repeated at hourly intervals throughout the day and interpolated to produce a continuous daily correction curve (Figure 4b). The process was then repeated for 1 day per month, and the daily correction curves for the rest of the year were interpolated to generate a continuous annual correction curve (Figure 4c).

The Federal Office of Topography swisstopo provides both a digital elevation model (DEM) and a digital surface model (DSM), the latter accounting for landscape elements such as vegetation and buildings. Both were tested for defining the correction curve, and the DSM yielded better results due to its inclusion of vegetation shading, which is important across most of the reach. Seasonal variation in shading was not considered, as only a single DSM acquired in spring (29–30 March 2019) was available. Radiation reaching vegetation is assumed to be fully blocked, regardless of vegetation density. This assumption has also been adopted in previous studies addressing similar objectives (e.g., Wawrzyniak et al., 2017). While some authors have incorporated vegetation density into shading calculations (Trimmel et al., 2018; Wade et al., 2024), these studies typically focus on short-term periods with limited vegetation dynamics, allowing for a fixed representation. Year-round simulations would require seasonally resolved vegetation data, which remain difficult to obtain. A time-invariant surface was therefore adopted as a consistent and operationally robust choice, but this assumption should be considered when interpreting the results.

Both the DEM and the DSM are provided as raster grids with a resolution of 0.5 m. Although attempts were made to compute the shading curve with a coarser resolution, this resulted not only in higher uncertainty but also in an underestimation of the shading effect due to its failure to capture small and sharp elements (Figure S1 in Supporting Information S1).

To account for variations in river width, vegetation, and channel orientation along the study reach, a test was conducted by dividing the reach into seven segments and applying the correction factor methodology to each one

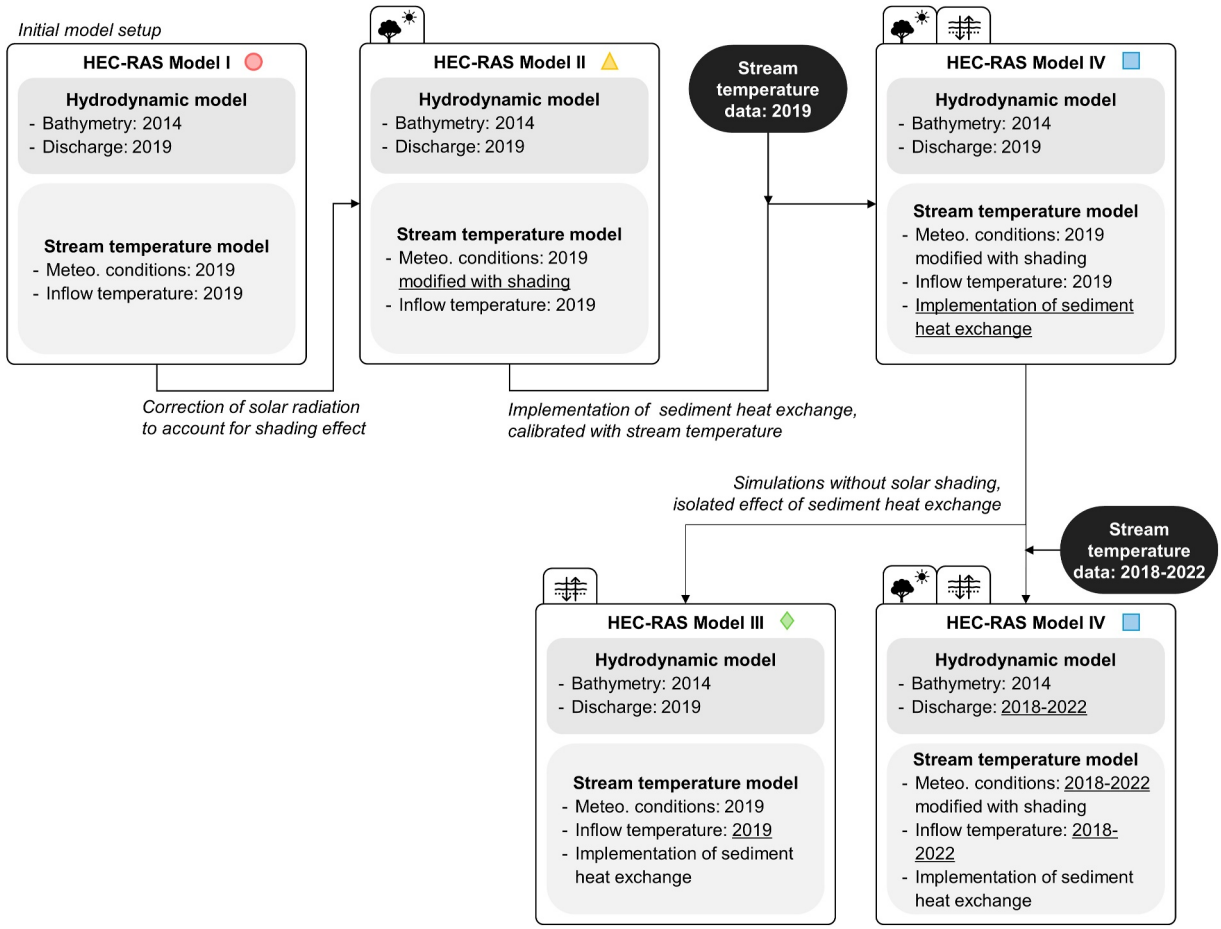

Figure 3. Developed methodology and model structures used in the study.

(Text S1 in Supporting Information S1). Although the resulting correction curves differed between segments (Figure S2 in Supporting Information S1), this locally refined approach had a negligible effect on simulation results (Figure S3 in Supporting Information S1). Consequently, the simulations considering shading effect reported in this paper were all conducted with an overall correction curve, computed over the entire reach, based on a DSM with a 0.5 m resolution.

2.5. Objective Functions to Describe Model Performance

2.5.1. Statistical Functions

The statistical functions given in Equations 6–10 are used to assess agreement between model results and measured stream temperature (Equation 10; Gupta et al., 2009).

$$\text{Mean absolute error: } \text{MAE} = \frac{1}{n}\sum_{i=1}^{n}|(x_{s,i} - x_{o,i})| \tag{6}$$

$$\text{Linear correlation coefficient: } R = \frac{Cov_{so}}{\sigma_s \cdot \sigma_o} \tag{7}$$

$$\text{Relative variability: } \alpha = \frac{\sigma_s}{\sigma_o} \tag{8}$$

$$\text{Relative bias: } \beta = \frac{\mu_s}{\mu_o} \tag{9}$$

19447973, 2025, 9, Downloaded from https://agupubs.onlinelibrary.wiley.com/doi/10.1029/2024WR038860 by Schweizerische Akademie Der, Wiley Online Library on [26/09/2025]. See the Terms and Conditions (https://onlinelibrary.wiley.com/terms-and-conditions) on Wiley Online Library for rules of use; OA articles are governed by the applicable Creative Commons License

$$\text{Kling} - \text{Gupta efficiency: } \text{KGE} = 1 - \sqrt{(R-1)^2 + (\alpha-1)^2 + (\beta-1)^2} \quad (10)$$

With n as the total number of time-steps, $x_{s,i}$ and $x_{o,i}$ as simulated and observed value at time-step i, Cov_{so} as covariance between simulated and observed values, σ_s and σ_o as standard deviation of the simulated and observed time-series, μ_s and μ_o as mean of the simulated and observed time-series.

The optimal value for MAE is 0, while a perfect agreement for the other statistical indicators is characterized by a value of 1. These functions can be applied to a measure of any duration greater than the minimum model time-step, so ranging from sub-hourly to multi-year durations.

2.5.2. Purpose-Driven Indicators

Further to classical statistical functions, the necessity to reproduce stream temperature distributions and patterns that are relevant for river management was recognized and "purpose-driven" indicators were derived.

Thermopeaking alteration in Switzerland is primarily evaluated using two indicators: the 90th percentile of the observed daily amplitude $AT90_o$ (°C) and the 90th percentile of the maximal observed daily gradient $TT90_o$ (°C/h) (OFEV, 2017a). Model performance is assessed by comparing these indicators between simulated and observed time-series.

The health of aquatic ecosystems is linked to the frequency distribution of stream temperature rather than overall statistical values. The number of days with an average stream temperature above 15°C is important ($N15°_o$), as it is correlated with the prevalence of proliferative kidney disease among fishes (OFEV, 2017b).

In subsequent tables and figures, the synthetic expression $AT90$, $TT90$, and $N15°$ will always refer to the actual difference between the signature of the simulated (subscript s) and observed (subscript o) time-series, expressed as:

$$AT90 = AT90_s - AT90_o \quad (11)$$

$$TT90 = TT90_s - TT90_o \quad (12)$$

$$N15° = N15°_s - N15°_o \quad (13)$$

2.6. Model Setup and Calibration

The evolution of the model across the different steps is illustrated in Figure 3. These steps aimed to test (a) a correction of raw solar radiation measured at the meteorological station using a shading model, and (b) the inclusion of a sediment temperature model to account for sediment-water heat exchange. Their individual and combined effects were evaluated through four model configurations:

(I) default model setup;
(II) default with shading correction;
(III) default with sediment temperature modeling; and
(IV) default with shading correction and sediment temperature modeling.

The initial model setup followed the HEC-RAS water temperature model described in Section 2.2, with driving factors (bathymetry, inflow discharge and temperature, and atmospheric conditions) informed by the data presented in Section 2.3.1. Model II incorporated solar radiation corrected using the shading method detailed in Section 2.4.

In Model IV, the sediment temperature module (Section 2.2) was activated. A dedicated calibration was carried out to address the limited knowledge of sediment properties and their influence on model performance. Since the first four terms of Equation 4 are constant and appear together in the heat flux calculation, they were combined into a single calibration parameter. Specifically, fixed values were assigned to three of these terms (h_2, ρ_s, and C_{ps}, values in Table 2), while only α_s was varied during calibration. Four sediment-related parameters were thus considered: thermal diffusivity (α_s) and the three coefficients describing the boundary temperature condition (T_{sed}). Two additional parameters were also included in the calibration, Manning's roughness coefficient (n) and a

19447973, 2025, 9, Downloaded from https://agupubs.onlinelibrary.wiley.com/doi/10.1029/2024WR038860 by Schweizerische Akademie Der, Wiley Online Library on [26/09/2025]. See the Terms and Conditions (https://onlinelibrary.wiley.com/terms-and-conditions) on Wiley Online Library for rules of use; OA articles are governed by the applicable Creative Commons License

19447973, 2025, 9, Downloaded from https://agupubs.onlinelibrary.wiley.com/doi/10.1029/2024WR038860 by Schweizerische Akademie Der, Wiley Online Library on [26/09/2025]. See the Terms and Conditions (https://onlinelibrary.wiley.com/terms-and-conditions) on Wiley Online Library for rules of use; OA articles are governed by the applicable Creative Commons License

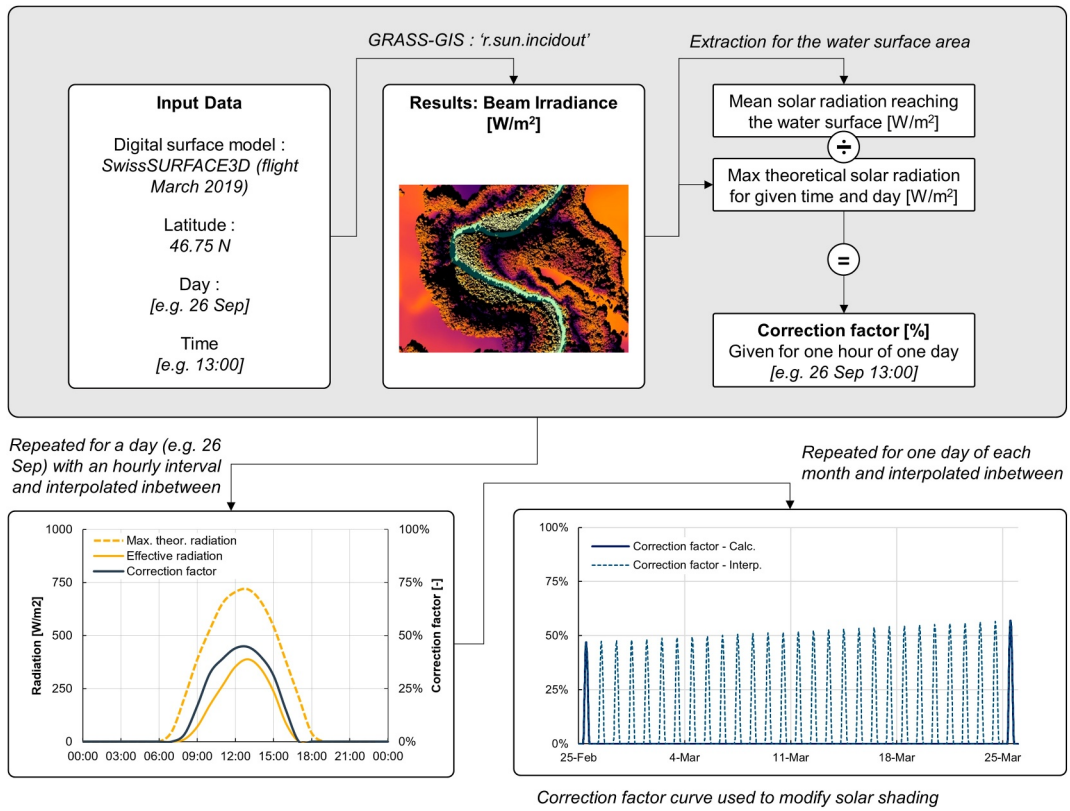

Figure 4. Flowchart of the methodology used to compute the correction curve applied to raw solar radiation data to account for shading effects.

longitudinal dispersion multiplier (m), due to their potential influence on the dynamics of thermal waves in the model. Model performance during calibration was evaluated using both classical statistical indicators and purpose-driven metrics, as outlined in Section 2.5. Calibration was conducted on Model IV (including shading correction) for the year 2019. The resulting parameter values, assumed constant in space and time, are listed in Table 2. Further details on the calibration strategy and evaluation are provided in Text S2 and Figures S4–S7 in Supporting Information S1.

Table 2
Parameters Value Used in the Model and Comparison to Reference Values for Water and Sediment Material From Literature [a](Chapra et al., 2008); [b](Gerecht et al., 2011)

Parameter		Unit	Model value	Water	Sediment material
Fixed parameter					
Layer thickness	h_2	[m]	2.0		
Bulk density	ρ_s	[kg/m3]	2,240	1,000 [a]	1,500–2,700[a]
Specific heat capacity	C_{ps}	[J/kg/°C]	1,670	4,180 [a]	800–2,200[a, b]
Calibrated parameter					
Manning's roughness	n	[–]	0.06		
Dispersion multiplier	m	[–]	0.75		
Thermal diffusivity	α_s	[m²/day]	1.5	0.012 [a]	0.03–0.11[a, b]
BC weight of fixed average	w_1	[–]	0.4		
BC weight of moving average	w_2	[–]	0.7		
BC moving average duration	Δt	[days]	70		

10.1029/2024WR038860

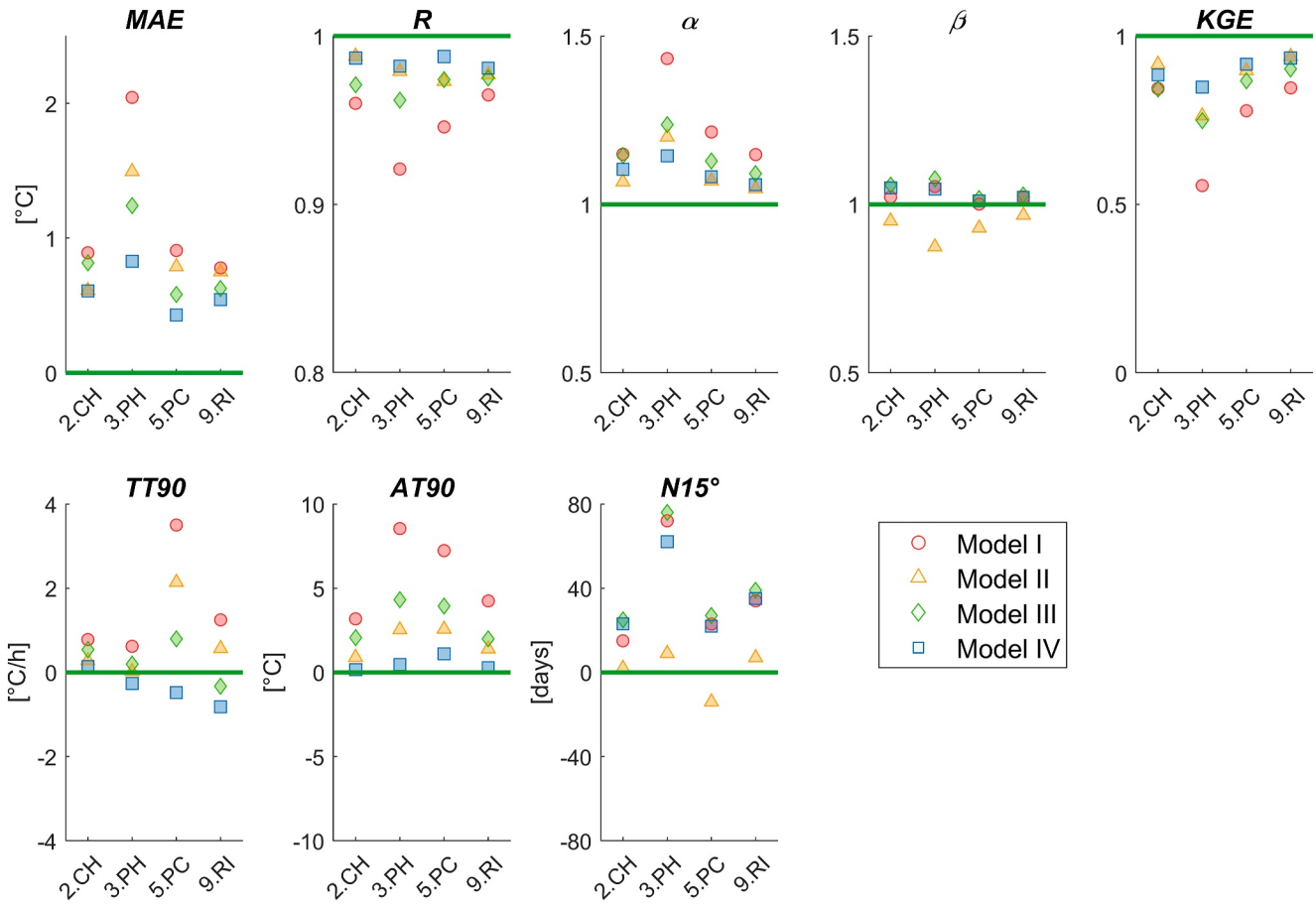

Figure 5. Comparison between the four models for the eight objective functions at four sections (Figure 1). The green line represents the perfect agreement.

To assess the model's temporal transferability, Model IV was run for four additional years (2018, 2020, 2021, and 2022) as part of a split-sample validation. Once sediment properties were calibrated, Model III was run with the sediment temperature module activated but using raw solar radiation data, in order to isolate the effect of sediment heat exchange.

3. Results

3.1. Model I: Initial Model

An example of time-series for two sections over a 10-day period in May is presented in Figure 6, where the results of Model I are represented as reference for the successive models. For the calibration year 2019, the mean absolute error (*MAE*) of the Model I ranges from 0.8 to 2.1°C, while the Kling-Gupta Efficiency (*KGE*) varies between 0.55 and 0.85 across the four sections considered (Figure 5). Upon closer examination of the model's bias and variability, it becomes visible that a slight tendency to predict warmer temperatures, ranging from 1.01 to 1.05 in relative bias (meaning average temperature is overestimated by 1%–5%), coupled with a high relative variability ranging from 1.15 to 1.40 (standard deviation is overestimated by 15%–40%). Regarding thermopeaking indicators, both gradients (*TT90*) and amplitudes (*AT90*) are excessively high. The count of days with an average temperature exceeding 15°C is also overestimated, with *N15°* varying from 15 to 72 days for the year 2019.

3.2. Model II: Influence of Shading

Comparing the performance between Models I and II for the calibration year 2019 allows for the assessment of the impact of the shading effect versus the full measured radiation. In Model II, *MAE* varies from 0.6 to 1.5°C, corresponding to an average reduction of 19% as compared to Model I, while *KGE* ranges from 0.76 to 0.94,

19447973, 2025, 9, Downloaded from https://agupubs.onlinelibrary.wiley.com/doi/10.1029/2024WR038860 by Schweizerische Akademie Der, Wiley Online Library on [26/09/2025]. See the Terms and Conditions (https://onlinelibrary.wiley.com/terms-and-conditions) on Wiley Online Library for rules of use; OA articles are governed by the applicable Creative Commons License

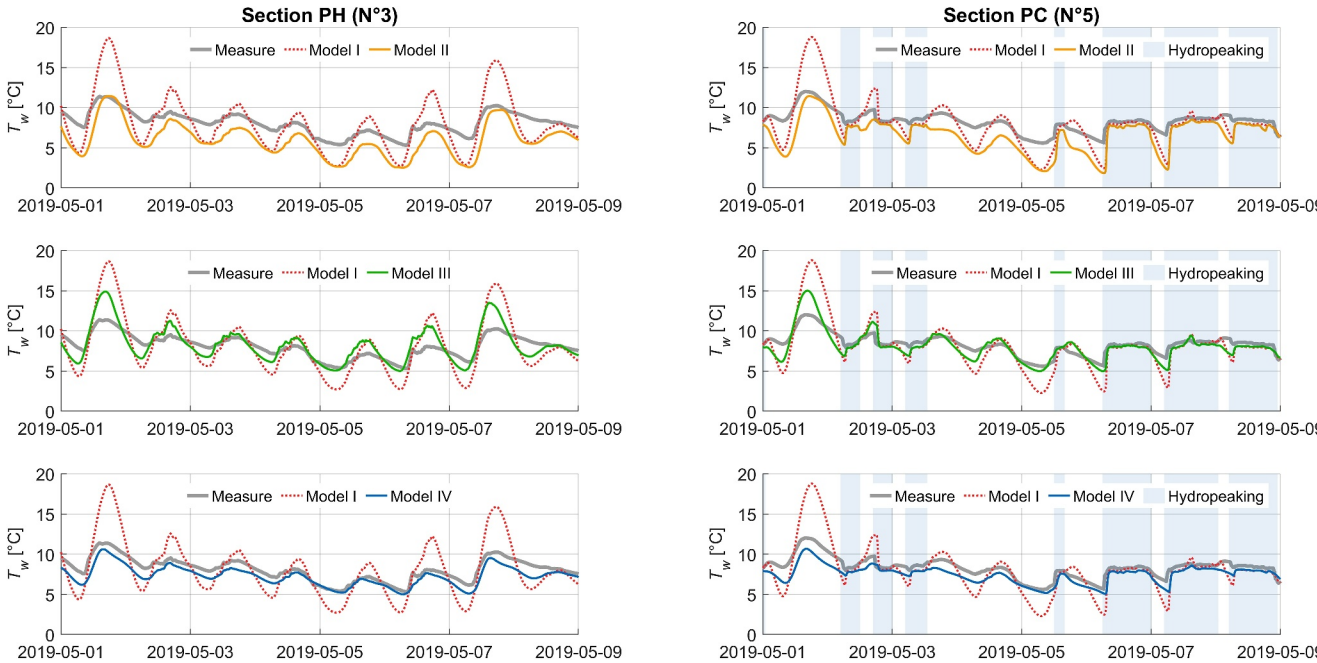

Figure 6. Comparison between measured stream temperature and results of the four models for a 10-day period in spring 2019.

corresponding to an average increase of 18%. The bias is now less than 1, with values between 0.87 and 0.97, characterizing a model that, on average, underestimates the temperature. The relative variability, although remaining above 1, is reduced to values between 1.05 and 1.20.

Regarding thermopeaking indicators, gradients are now closer to measured values, with a deviation ranging from 0 to 2.1°C/h. Amplitudes are also closer to measurements with a slight overestimation ranging from 0.9 to 2.6°C. The count of days with an average temperature exceeding 15°C is better estimated, with values ranging from −9 to +14 days. The consideration of solar shading thus leads to a significant improvement in all indicators, except for the relative bias that is overcorrected.

3.3. Model III: Influence of Water-Sediment Heat Exchange

The comparison of the performance between Models I and III for the calibration year 2019 shows the effect of including the sediment-water heat flux in the model. Although the sediment layer parameters were calibrated in the model considering the solar shading correction, here the models without the shading correction are compared for consistency. In Model III, *MAE* varies from 0.6 to 1.2°C, corresponding to an average reduction of 26% relative to Model I, while *KGE* ranges from 0.75 to 0.90. Among the statistical functions, solely the positive bias is deteriorated with values ranging now between 1.02 and 1.08. Regarding thermopeaking indicators, gradients are now closer to measured values, with deviations ranging from −0.3 to +0.8°C/h. Amplitudes are still overestimated but within a range of 2.0–4.3°C. The count of days with an average temperature exceeding 15°C is overestimated again, even slightly higher than for Model I. Overall, the consideration of water-sediment heat flux improves the model's performance for most functions, except that it leads to a warmer model with a higher positive bias and an overestimation of the *N15°* indicator.

3.4. Model IV: Influence of Combined Modifications

The comparison between Model I and Model IV for the calibration year 2019 shows that the combination of the shading correction on the solar radiation and the additional water-sediment heat flux significantly enhances model performance. The *MAE* is reduced to 0.4–0.8°C. Additionally, *KGE* varies from 0.85 to 0.93. The bias remains slightly positive, with values similar to those of the initial Model I (1.01–1.05). Though still overestimated, the relative variability is reduced to values ranging from 1.06 to 1.1.

19447973, 2025, 9, Downloaded from https://agupubs.onlinelibrary.wiley.com/doi/10.1029/2024WR038860 by Schweizerische Akademie Der, Wiley Online Library on [26/09/2025]. See the Terms and Conditions (https://onlinelibrary.wiley.com/terms-and-conditions) on Wiley Online Library for rules of use; OA articles are governed by the applicable Creative Commons License

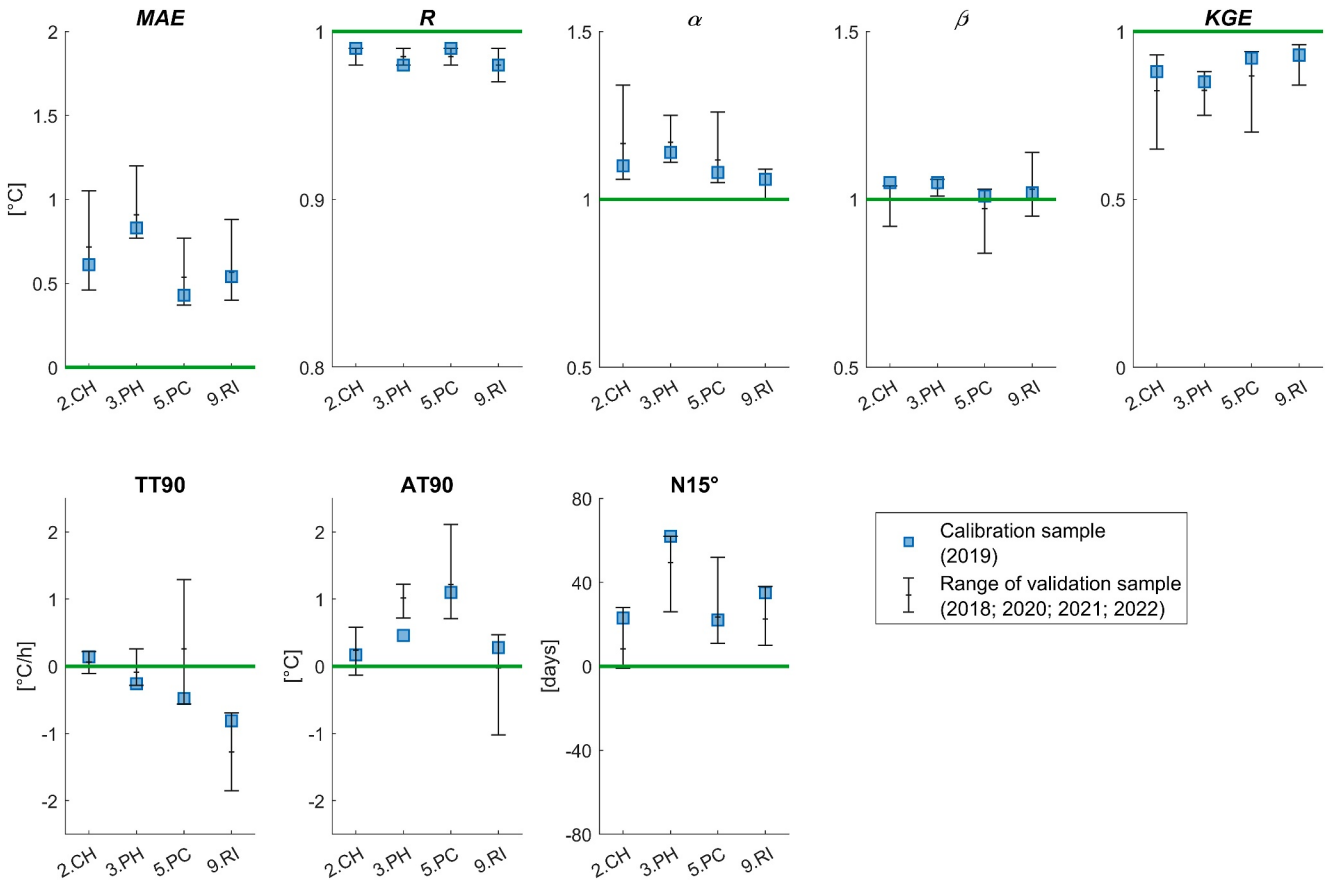

Figure 7. Evaluation of model's temporal transferability by comparing model performance for calibration and validation data set.

Concerning thermopeaking indicators, gradients are now closer for both upstream sections and only slightly underestimated for both downstream sections. Amplitudes align more closely with measurements, showing a slight overestimation ranging from 0.17 to 1.10°C. However, the count of days with an average temperature exceeding 15°C is still overestimated for most sections, ranging from 22 to 62 days.

3.5. Validation

Among the four models, Model IV yielded the most satisfying results for the calibration year 2019. Its performance was then tested over four validation years (2018, 2020, 2021 and 2022). Figure 7 presents the range of results obtained for the model performance during the validation years in comparison to the calibration period. Generally, the model's performance does not exhibit significant degradation during the validation years, except for *TT90* for Section 9.RI and *AT90* for Section 3.PH.

4. Discussion

In this study, shading correction in the model yielded a notable improvement and seems to be the most important process needed to reproduce the stream temperature data sets. This outcome aligns with findings in the literature, which identify solar radiation as a major component of the river heat budget (Dugdale et al., 2024; Hannah et al., 2004; Wawrzyniak et al., 2017; Webb & Zhang, 1997). The improvement in model accuracy associated with this process likely reflects the specific characteristics of the study site, where the river flows through a gorge densely covered with vegetation. Computing shading in a GIS presents several challenges: it requires high spatial resolution to capture local effects (Dugdale et al., 2020), consideration of distant topographic obstructions (Bode et al., 2014), accurate representation of daily and seasonal changes in solar angle (Loicq et al., 2018), and accounting for seasonal variations in vegetation cover (Dugdale, Malcolm, & Hannah, 2019). In this study, temporal variability was simplified by interpolating shading at hourly and monthly intervals, and a unique DSM was used.

19447973, 2025, 9, Downloaded from https://agupubs.onlinelibrary.wiley.com/doi/10.1029/2024WR038860 by Schweizerische Akademie Der, Wiley Online Library on [26/09/2025]. See the Terms and Conditions (https://onlinelibrary.wiley.com/terms-and-conditions) on Wiley Online Library for rules of use; OA articles are governed by the applicable Creative Commons License

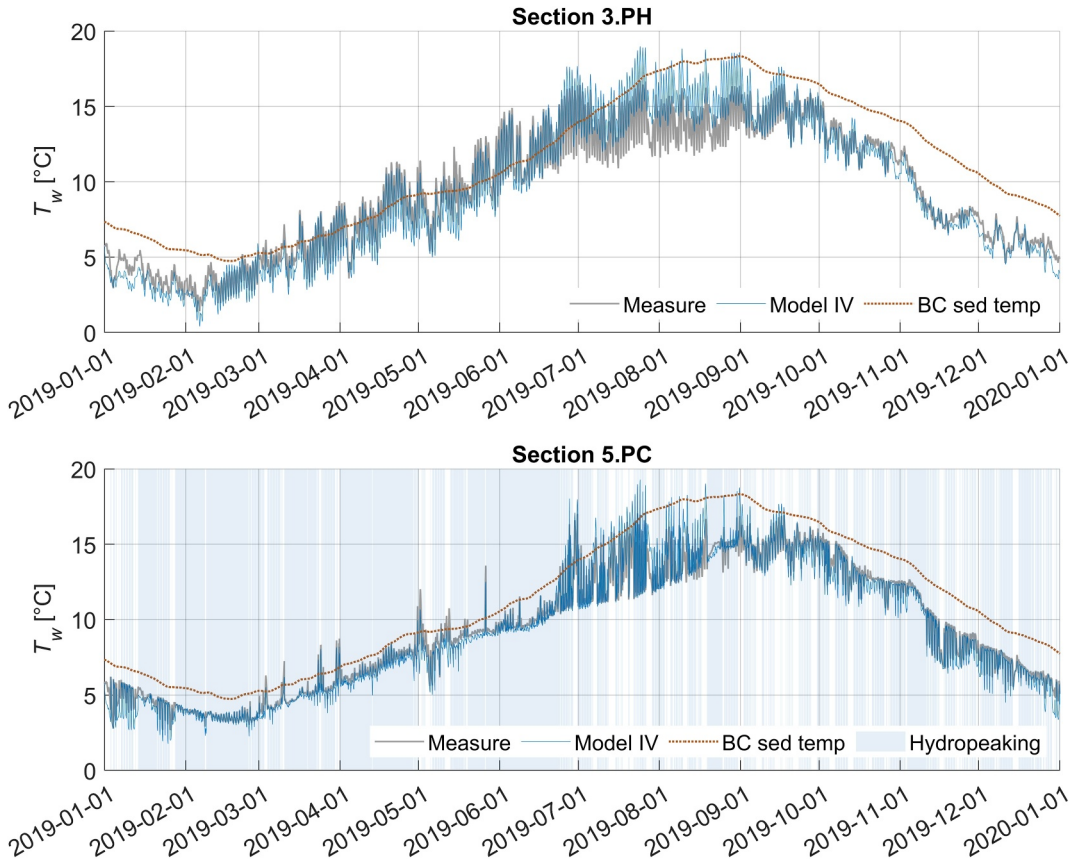

Figure 8. Yearly time-series of measured and modeled stream temperature (Model IV). The sediment layer boundary condition temperature is indicated by a dotted line.

Our results indicate that, for long-term simulations, the lack of data on seasonal vegetation changes is not necessarily a limiting factor for achieving good model performance. Spatially, a single correction factor was applied uniformly along the reach. Although channel orientation can influence shading (Garner et al., 2017), the limited variability along the studied reach, combined with continuous flow, suggests that a reach-scale representation is sufficient and that fine-scale variability in shading has limited impact on model results. The divergence identified between solar radiation measurements at the meteorological station and riverside conditions may also apply to other atmospheric variables.

In this study, air temperature and relative humidity were measured at three river-side stations and compared to data from the meteorological station. The differences were limited, and their impact on model results was negligible. However, in other contexts, correcting meteorological inputs has been shown to improve model performance (Beaupré et al., 2020), highlighting the importance of assessing the representativeness of such data in similar applications. While shading improved most performance metrics compared to the initial model, it also reduced the relative bias below 1 (Figure 5), indicating that simulated temperatures were slightly too low on average. This is because shading correction lowers daytime temperatures without affecting nighttime conditions (Figure 6, top), preserving the model's tendency to overestimate nocturnal cooling, particularly during winter and spring when air temperatures are low (Figure 9, bottom). This suggests that additional processes are needed to improve the representation of nighttime thermal dynamics.

The inclusion of water-sediment heat exchanges also improved model performance by accounting for thermal buffering in the riverbed. Implementing this process is constrained by the lack of direct data on sediment thermal properties. The sediment heat flux depends on several physical parameters—sediment density (ρ_s), specific heat capacity (C_{ps}), layer thickness (h_2), and thermal diffusivity (α_s)—which appear jointly in the flux expression. This reduces calibration complexity, as only one effective parameter needs to be adjusted, but limits the physical

19447973, 2025, 9, Downloaded from https://agupubs.onlinelibrary.wiley.com/doi/10.1029/2024WR038860 by Schweizerische Akademie Der, Wiley Online Library on [26/09/2025]. See the Terms and Conditions (https://onlinelibrary.wiley.com/terms-and-conditions) on Wiley Online Library for rules of use; OA articles are governed by the applicable Creative Commons License

10.1029/2024WR038860

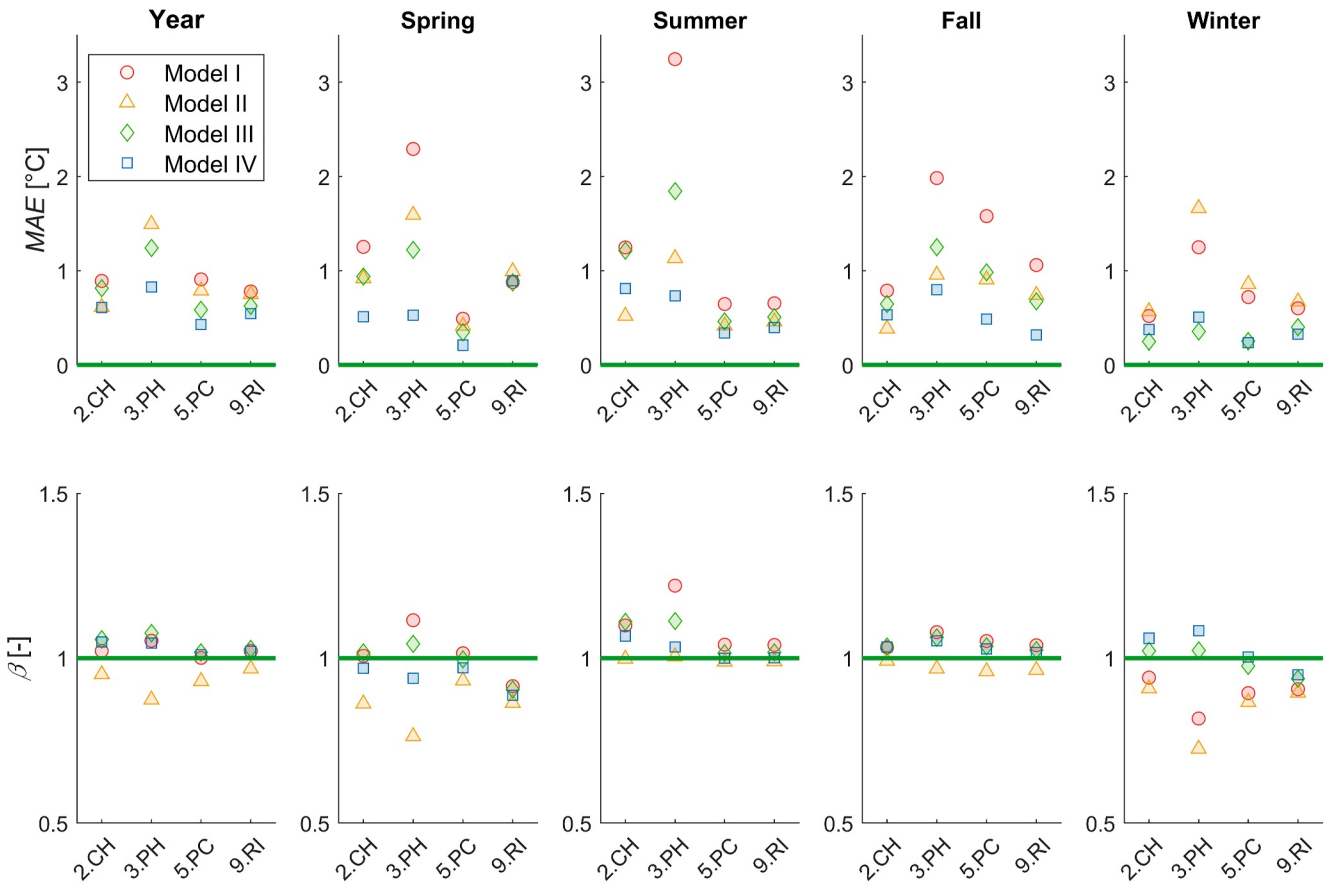

Figure 9. Comparison of model performance for the four models based on two indicators, computed at the yearly scale (2019) and for the different seasons.

interpretability of individual terms. In this study, ρ_s, C_{ps}, and h_2 were fixed to represent a saturated layer composed of 75% sediment and 25% water, with h_2 set at 2 m, and only α_s was varied during calibration. The resulting calibrated diffusivity (1.5 m^2/day) is substantially higher than typical reference values for sediments (0.03–0.11 m^2/day), likely reflecting the need to account for advective heat fluxes, which are not explicitly represented in the model. In unregulated rivers, thermal damping depths typically range from 0.10 to 0.25 m (Chapra et al., 2008; Gerecht et al., 2011; Sawyer et al., 2009). In contrast, regulated rivers experience stage fluctuations that enhance hyporheic mixing, with observed thermal signals at depths exceeding 1 m (Boutt & Fleming, 2009; Sawyer et al., 2009). The propagation of thermal signals beyond expected damping depths also indicates the presence of advective transport (Gerecht et al., 2011). Given the difficulty of separately representing all thermal processes at the streambed interface, they are often treated as a single integrated exchange term in modeling approaches (Dugdale et al., 2017). These considerations support the assumption of a thicker active sediment layer and elevated diffusivity in the model (Table 2). Assuming constant sediment layer properties in space and time is a notable limitation, as studies have shown that these properties can vary both along the river reach and over time (Keery et al., 2007; Trimmel et al., 2018; Zhang & Johnson, 2016). This heterogeneity is particularly relevant in this case, where the model spans multiple years in a regulated river subject to chronic sediment deficit, erosion, and artificial sediment replenishment. Yearly time series (Figure 8) suggest that the sediment temperature boundary condition helps capture realistic minimum temperatures in downstream sections, but tends to overestimate summer temperatures and underestimate winter temperatures in upstream areas. Assigning section-specific boundary conditions could improve spatial and temporal accuracy. However, while a more detailed calibration or direct measurement of sediment properties might enhance model performance, increasing model complexity could compromise transferability.

The improvement in model performance after calibration questions whether the sediment heat flux reflects actual riverbed processes or compensates for other mechanisms through calibration. While the implemented heat flux is

19447973, 2025, 9, Downloaded from https://agupubs.onlinelibrary.wiley.com/doi/10.1029/2024WR038860 by Schweizerische Akademie Der, Wiley Online Library on [26/09/2025]. See the Terms and Conditions (https://onlinelibrary.wiley.com/terms-and-conditions) on Wiley Online Library for rules of use; OA articles are governed by the applicable Creative Commons License

19447973, 2025, 9, Downloaded from https://agupubs.onlinelibrary.wiley.com/doi/10.1029/2024WR038860 by Schweizerische Akademie Der, Wiley Online Library on [26/09/2025]. See the Terms and Conditions (https://onlinelibrary.wiley.com/terms-and-conditions) on Wiley Online Library for rules of use; OA articles are governed by the applicable Creative Commons License

physically-based, its interpretation warrants caution. First, the physical parameters describing the sediment layer are aggregated in the heat flux expression and cannot be individually identified or compared with reference values. Second, the results show that including sediment heat exchange improved model performance similarly in both upstream and downstream sections (Figure 6). However, the high thermal diffusivity and large sediment layer thickness used in the model are more easily justified downstream, where hyporheic exchanges are enhanced by flow fluctuations from hydropeaking. Such exchanges are less expected in upstream sections with relatively stable flows (Burkholder et al., 2008). This suggests that the calibrated heat flux may also encompass other effective thermal inertia processes not explicitly modeled. These types of conceptual representations are common in process-based modeling (Beven, 1989; Clark et al., 2015), particularly for processes that are difficult to characterize (Wade et al., 2024), but their conceptual nature should be acknowledged and their physical interpretation approached with caution. Finally, in addition to including sediment heat exchange, Models III and IV incorporated updated values for roughness ($n = 0.06$ vs. 0.045) and longitudinal dispersion ($m = 0.75$ vs. 1), both calibrated over wide tested ranges. However, the retained values were too close to the initial ones to have a major impact on results, and their influence was an order of magnitude smaller than that of the sediment heat exchange.

Multiplying the components in a process-based model increases the number of parameters, equations, and the data requirements needed to account for the parameter variability (Beven, 2018). To maintain model parsimony, certain processes (precipitation, groundwater inflow, wind) were excluded from the calibrated model as they were determined to have minimal influence on stream temperature in this specific study.

Energy advected by precipitation is rarely considered in the heat budget (Caissie, 2006; Dugdale et al., 2017). Rainfall can influence stream temperature via discharge fluctuations. In this case, the highly regulated river experiences only minor discharge variations during precipitation due to the presence of dams and power plants that regulate the flow; the effects are limited primarily to direct precipitation. A comparison was carried out for the years 2018 and 2019 between the cumulated inflow volumes (dam releases, power plant discharge, and tributaries) and the integrated discharge measured 2 km downstream of the study reach at a federal hydrometric station. The missing volume attributed to direct runoff accounted for only 0.4% and 0.9%, respectively.

Groundwater inflows can also influence stream temperature in gaining reaches (Arrigoni et al., 2008; Constantz, 1998). Groundwater inflow was modeled at three local sections where sources with known discharges feed the river. However, since the total discharge from these sources accounts for less than 5% of the residual flow (Thierrin, 1990), their effect on temperatures was practically negligible. While such discharges of groundwater inflows might be locally important for thermal refuges (Dugdale et al., 2013; Kurylyk et al., 2014), their effect on average temperature in a reach-scale model is limited. Wind can significantly impact the heat budget through latent and sensible heat fluxes (Hannah et al., 2008; Maheu et al., 2014).

The effect of wind was tested in the model using wind velocity data measured at the meteorological station. Its impact on modeled stream temperature was negligible. Furthermore, actual wind velocity at the river surface is expected to have even less influence due to the topography and vegetation along the river, which reduce exposure.

Model IV performance exhibits clear seasonal and spatial variability, reflecting the influence of different dominant thermal processes. As shown in Figure 9, *MAE* is lower in winter due to reduced thermal variability, and while the annual relative bias (β) is above 1 for all sections, it drops below one in some cases during spring and winter. Spatially, Section 3.PH displays higher errors and bias, likely due to its intermediate location and reduced influence from either lake temperature or hydropeaking releases. In terms of thermal gradients, Model IV reproduces *TT90* accurately for upstream sections (2.CH and 3.PH), but underestimates it for downstream sections (5.PC and 9.RI), which experience stronger hydropeaking-induced fluctuations (Figure 5). These results highlight the importance of assessing model performance over both time and space, as simplifications may have uneven effects. They also caution against generalizing model performance from a single section or limited calibration period.

The improvement in model performance from Model I to Model IV highlights the importance of targeted corrections when using generic process-based stream temperature models. These refinements require appropriate calibration data, ideally covering seasonal and short-term variability. In regulated rivers, this means acquiring continuous time-series rather than spot measurements. Although this study used a large and distributed data set, similar performance could likely be achieved with 1–2 years of continuous measurements on a limited number of cross-sections. Remote sensing, while valuable for characterizing thermal heterogeneity (Casas-Mulet

19447973, 2025, 9, Downloaded from https://agupubs.onlinelibrary.wiley.com/doi/10.1029/2024WR038860 by Schweizerische Akademie Der, Wiley Online Library on [26/09/2025]. See the Terms and Conditions (https://onlinelibrary.wiley.com/terms-and-conditions) on Wiley Online Library for rules of use; OA articles are governed by the applicable Creative Commons License

et al., 2020; Dugdale, 2016; Dugdale, Kelleher, et al., 2019), lacks the temporal resolution needed for such applications. In contrast, deploying temperature sensors is relatively simple on accessible catchment and less demanding than flow measurements, making it a practical solution for many river monitoring projects.

Although Model IV outperforms other models based on standard statistical metrics such as *MAE* and *KGE* (Figure 5), purpose-driven indicators like *TT90* and *N15°* provide less clear results. The choice of evaluation metrics can significantly influence model assessment, as commonly used indicators may not adequately reflect a model's ability to capture relevant hydrological signatures (Todorović et al., 2022). Evaluation therefore requires consideration of multiple indicators (Ritter & Muñoz-Carpena, 2013). In the context of environmental impacts, accurate representation of indicators such as *TT90* and *AT90* provides a more meaningful basis for assessing model fitness-for-purpose (Beven & Lane, 2022). In this study, *AT90* was well reproduced overall, while *TT90* showed stronger agreement for upstream sections than for downstream areas affected by hydropeaking (Figure 5). Several factors help explain this: (a) higher absolute gradients downstream inflate perceived discrepancies; (b) expressing *TT90* in °C/h amplifies differences due to the 10-min timestep (a multiplication factor of 6), which diminishes when longer time intervals are used; and (c) hydropeaking discharges were only available at hourly resolution, limiting accuracy in reproducing abrupt thermal changes. Despite these limitations, Model IV accurately represents the timing and physical origin of peak gradients, in contrast to Models I and II, where *TT90* peaks result from solar radiation and occur at incorrect times. This aligns with the principle of achieving the right results for the right reasons in model validation (Kirchner, 2006). Moreover, under the Swiss hydropeaking mitigation framework, which categorizes river segments based on thermal criteria, Model IV correctly classified 100% of upstream segments and achieved 90% agreement for hydropeaking-affected downstream segments over 2018–2022. This supports the model's robustness and relevance for operational decision-making.

Another aspect of fitness-for-purpose validation is the model's temporal transferability, as a model may be invalidated despite strong performance during the calibration period (Hrachowitz et al., 2014). Figure 7 shows that the model performance metrics obtained for the calibration year (2019) fall within the range of variation observed during the validation period (2018 and 2020–2022), although they are often slightly better; for instance, the *MAE* for 2019 is lower than the average *MAE* for the other years. This robust transferability can be attributed to the physically based shading correction, the intentionally limited complexity of the sediment heat exchange module, and the extensive data set used to support calibration.

Until now, the discussion of output error has focused on model structure and process representation; however, additional sources of uncertainty must be acknowledged as methodological limitations. These include uncertainties associated with temperature probes during stream temperature measurements, potential inaccuracies due to the oversight of thermal variations within the stream, and the assumption that the measured temperature adequately represents the entire section (1D). Additionally, the difference in temporal resolutions introduces another element of error, with stream temperature modeling using a 10-min timestep, while discharge data are available at a 1-hr resolution.

In addition to its immediate applications, this study offers valuable outcomes for both stream temperature research and river management. Recent efforts have focused on developing machine learning models for stream temperature prediction. While promising, these approaches still face challenges regarding robust spatiotemporal architectures (Nearing et al., 2021). Process-guided strategies—such as pre-training deep learning models on the outputs of process-based models—have shown potential (Topp et al., 2023), but these developments underscore that advancing spatially explicit process-based models remains both relevant and necessary. Furthermore, progress in high-resolution thermal modeling may create new opportunities for hydrologic applications. Facing limited data availability and growing demands, the hydrologic community is increasingly turning to alternative data sources (Stadnyk & Holmes, 2023). Temperature time series are easier to collect than discharges and have already been used as tracers to investigate groundwater-surface water interactions (Constantz, 2008; Kurylyk et al., 2017). With access to accurate, high-frequency stream temperature models, it becomes possible to better represent processes such as flow partitioning, residence times, or flow path identification, especially in complex or regulated systems. In the meantime, this study demonstrates that process-based modeling remains a highly effective tool for river management.

When properly calibrated, a single model was able to predict stream temperature with a $MAE < 1.0$°C across several cross-sections, both with and without hydropeaking, over a 22-km reach and multiple years, all while maintaining fine temporal resolution. Although comparable performance levels have been reported in prior

studies, these often focused on a single site or shorter reach (Gallice et al., 2016; Garner et al., 2017; Wawrzyniak et al., 2017), shorter time spans (Garner et al., 2017; Wade et al., 2024; Wawrzyniak et al., 2017; Woltemade & Hawkins, 2016), or coarser temporal resolution (Bourqui et al., 2011; Gatien et al., 2023; Michel et al., 2022). These capabilities are particularly valuable for assessing the impacts of climate change, hydropower mitigation strategies, or for enhancing the integration of stream temperature in habitat modeling (Antonetti et al., 2023; Ouellet et al., 2020).

5. Conclusions

This study demonstrates that robust stream temperature simulations are achievable in regulated rivers, including thermopeaking conditions, using a process-based model supported by high-quality, spatially distributed data. With the calibration of only a few parameters, the model reproduced complex thermal dynamics across several years and river sections, maintaining fine temporal resolution with a mean absolute error below 1°C. Key improvements resulted from including two dominant processes: solar shading and sediment-water heat exchange. A simple GIS-based shading correction substantially improved performance, highlighting the critical role of solar radiation. Although it aggregates several unresolved processes, the sediment heat flux provides a practical and effective way to represent streambed thermal inertia in the model. The model's transferability over time and its evaluation using both statistical and purpose-driven indicators confirm its relevance for operational applications. In particular, it meets the requirements of environmental management frameworks by reproducing both long-term trends and short-term fluctuations, two temporal scales essential for aquatic ecosystem health. This work provides a practical tool for guiding decisions on hydropower regulation, thermal water uses, and climate adaptation strategies. Its ability to resolve spatial and temporal thermal variability makes it suitable for scenario-based simulations assessing the thermal effects of river restoration projects, hydropower or hydropeaking mitigation strategies, and long-term changes in riparian vegetation. These applications can support planning and prioritization of interventions in river systems facing increasing pressures from climate change and human activities.

Future research could focus on integrating biological or socio-economic response models to evaluate trade-offs between thermal regimes, ecological health, and energy production. In addition, improving the representation of sediment processes and testing model transferability across diverse river systems would further enhance its robustness and applicability.

Data Availability Statement

The stream temperature data set used for model calibration, validation and model performance assessment in the study is available on Zenodo at https://doi.org/10.5281/zenodo.15213206 (Dorthe et al., 2025). Meteorological data were downloaded from the MeteoSwiss Open Data portal (https://www.meteoswiss.admin.ch/services-and-publications/service/open-data.html; MeteoSwiss, 2025).Discharge data for the two tributaries were obtained from the Swissrivers portal of the Canton of Fribourg (https://fribourg.swissrivers.ch; Swissrivers, 2025). The numerical modeling was carried out using HEC-RAS version 6.3, developed by the U.S. Army Corps of Engineers' Hydrologic Engineering Center (HEC, 2022) and freely available at https://www.hec.usace.army.mil/software/hec-ras/download.aspx. Discharge data from the hydropower operator are subject to usage restrictions, were provided solely for the purposes of this study, and cannot be publicly shared or redistributed.

Acknowledgments
This study was funded by Groupe E, Ribi SA ingénieurs hydrauliciens, School of Engineering and Architecture of Fribourg (HEIA-FR, Funding Ra&D), and Haute école spécialisée de Suisse occidentale (HES-SO). We thank the HEIA-FR technicians Elodie Moulin, Yanis Schaller, Dominique Delaquis, and (formerly) Bruno Spahni for the set-up of the in situ measurement equipment, as well as for the long-time and reliable operation of the latter. ChatGPT (OpenAI, 2024) was used to assist with the grammatical and stylistic revision of the manuscript. All content was reviewed and edited by the authors. Open access publishing facilitated by Universite de Lausanne, as part of the Wiley - Universite de Lausanne agreement via the Consortium Of Swiss Academic Libraries.

References

Abdi, R., Rogers, J. B., Rust, A., Wolfand, J. M., Philippus, D., Taniguchi-Quan, K., et al. (2021). Simulating the thermal impact of substrate temperature on ecological restoration in shallow urban rivers. *Journal of Environmental Management*, *289*, 112560. https://doi.org/10.1016/j.jenvman.2021.112560

Antonetti, M., Hoppler, L., Tonolla, D., Vanzo, D., Schmid, M., & Doering, M. (2023). Integrating two-dimensional water temperature simulations into a fish habitat model to improve hydro- and thermopeaking impact assessment. *River Research and Applications*, *39*(3), 501–521. https://doi.org/10.1002/rra.4043

Arrigoni, A. S., Poole, G. C., Mertes, L. A. K., O'Daniel, S. J., Woessner, W. W., & Thomas, S. A. (2008). Buffered, lagged, or cooled? Disentangling hyporheic influences on temperature cycles in stream channels. *Water Resources Research*, *44*(9). https://doi.org/10.1029/2007WR006480

Auer, S., Hayes, D. S., Führer, S., Zeiringer, B., & Schmutz, S. (2023). Effects of cold and warm thermopeaking on drift and stranding of juvenile European grayling (Thymallus thymallus). *River Research and Applications*, *39*(3), 401–411. https://doi.org/10.1002/rra.4077

Beaupré, L., St-Hilaire, A., Daigle, A., & Bergeron, N. (2020). Comparison of a deterministic and statistical approach for the prediction of thermal indices in regulated and unregulated river reaches: Case study of the Fourchue River (Québec, Canada). *Water Quality Research Journal*, *55*(4), 394–408. https://doi.org/10.2166/wqrj.2020.001

19447973, 2025, 9, Downloaded from https://agupubs.onlinelibrary.wiley.com/doi/10.1029/2024WR038860 by Schweizerische Akademie Der, Wiley Online Library on [26/09/2025]. See the Terms and Conditions (https://onlinelibrary.wiley.com/terms-and-conditions) on Wiley Online Library for rules of use; OA articles are governed by the applicable Creative Commons License

Benyahya, L., Caissie, D., St-Hilaire, A., Ouarda, T. B. M. J., & Bobée, B. (2007). A review of statistical water temperature models. *Canadian Water Resources Journal/Revue Canadienne Des Ressources Hydriques*, *32*(3), 179–192. https://doi.org/10.4296/cwrj3203179

Beven, K. (1989). Changing ideas in hydrology—The case of physically-based models. *Journal of Hydrology*, *105*(1), 157–172. https://doi.org/10.1016/0022-1694(89)90101-7

Beven, K. (2018). *Environmental modelling: An uncertain future?* CRC Press. https://doi.org/10.1201/9781482288575

Beven, K., & Lane, S. (2022). On (in)validating environmental models. 1. Principles for formulating a Turing-like Test for determining when a model is fit-for purpose. *Hydrological Processes*, *36*(10), e14704. https://doi.org/10.1002/hyp.14704

Birkel, C., Soulsby, C., Irvine, D. J., Malcolm, I., Lautz, L. K., & Tetzlaff, D. (2016). Heat-based hyporheic flux calculations in heterogeneous salmon spawning gravels. *Aquatic Sciences*, *78*(2), 203–213. https://doi.org/10.1007/s00027-015-0417-4

Bode, C. A., Limm, M. P., Power, M. E., & Finlay, J. C. (2014). Subcanopy Solar Radiation model: Predicting solar radiation across a heavily vegetated landscape using LiDAR and GIS solar radiation models. *Remote Sensing of Environment*, *154*, 387–397. https://doi.org/10.1016/j.rse.2014.01.028

Bourqui, M., Hendrickx, F., & Le Moine, N. (2011). *Long-term forecasting of flow and water temperature for cooling systems: Case study of the Rhone River, France* (Vol. 348, pp. 135–142). IAHS Publication.

Boutt, D. F., & Fleming, B. J. (2009). Implications of anthropogenic river stage fluctuations on mass transport in a valley fill aquifer. *Water Resources Research*, *45*(4). https://doi.org/10.1029/2007WR006526

Brunke, M., & Gonser, T. (1997). The ecological significance of exchange processes between rivers and groundwater. *Freshwater Biology*, *37*(1), 1–33. https://doi.org/10.1046/j.1365-2427.1997.00143.x

Brunner, G. W. (2016). *HEC-RAS river analysis system user's manual version 5.0* (Vol. 962). US Army Corps of Engineers.

Burkholder, B. K., Grant, G. E., Haggerty, R., Khangaonkar, T., & Wampler, P. J. (2008). Influence of hyporheic flow and geomorphology on temperature of a large, gravel-bed river, Clackamas River, Oregon, USA. *Hydrological Processes*, *22*(7), 941–953. https://doi.org/10.1002/hyp.6984

Caissie, D. (2006). The thermal regime of rivers: A review. *Freshwater Biology*, *51*(8), 1389–1406. https://doi.org/10.1111/j.1365-2427.2006.01597.x

Caissie, D., El-Jabi, N., & Turkkan, N. (2014). Stream water temperature modeling under climate change scenarios B1 & A2.

Caissie, D., Kurylyk, B. L., St-Hilaire, A., El-Jabi, N., & MacQuarrie, K. T. B. (2014). Streambed temperature dynamics and corresponding heat fluxes in small streams experiencing seasonal ice cover. *Journal of Hydrology*, *519*, 1441–1452. https://doi.org/10.1016/j.jhydrol.2014.09.034

Caissie, D., & Luce, C. H. (2017). Quantifying streambed advection and conduction heat fluxes. *Water Resources Research*, *53*(2), 1595–1624. https://doi.org/10.1002/2016WR019813

Caissie, D., Satish, M. G., & El-Jabi, N. (2005). Predicting river water temperatures using the equilibrium temperature concept with application on Miramichi River catchments (New Brunswick, Canada). *Hydrological Processes*, *19*(11), 2137–2159. https://doi.org/10.1002/hyp.5684

Casas-Mulet, R., Pander, J., Ryu, D., Stewardson, M. J., & Geist, J. (2020). Unmanned aerial vehicle (UAV)-based thermal infra-red (TIR) and optical imagery reveals multi-spatial Scale controls of cold-water areas over a groundwater-dominated riverscape. *Frontiers in Environmental Science*, *8*, 64. https://doi.org/10.3389/fenvs.2020.00064

Chapra, S. C., Pelletier, G. J., & Tao, H. (2008). Qual2K. A modeling framework for simulating river and stream water quality. Version, 2.

Clark, M. P., Nijssen, B., Lundquist, J. D., Kavetski, D., Rupp, D. E., Woods, R. A., et al. (2015). A unified approach for process-based hydrologic modeling: 1. Modeling concept. *Water Resources Research*, *51*(4), 2498–2514. https://doi.org/10.1002/2015WR017198

Cole, J. C., Maloney, K. O., Schmid, M., & McKenna, J. E. (2014). Developing and testing temperature models for regulated systems: A case study on the Upper Delaware River. *Journal of Hydrology*, *519*, 588–598. https://doi.org/10.1016/j.jhydrol.2014.07.058

Constantz, J. (1998). Interaction between stream temperature, streamflow, and groundwater exchanges in alpine streams. *Water Resources Research*, *34*(7), 1609–1615. https://doi.org/10.1029/98WR00998

Constantz, J. (2008). Heat as a tracer to determine streambed water exchanges. *Water Resources Research*, *44*(4). https://doi.org/10.1029/2008WR006996

Dorthe, D., Pfister, M., & Lane, S. (2025). Stream Temperature Data—Sarine River, Switzerland (2018–2022) [Dataset]. *Zenodo*. https://doi.org/10.5281/zenodo.15213206

Dugdale, S. J. (2016). A practitioner's guide to thermal infrared remote sensing of rivers and streams: Recent advances, precautions and considerations. *WIREs Water*, *3*(2), 251–268. https://doi.org/10.1002/wat2.1135

Dugdale, S. J., Bergeron, N. E., & St-Hilaire, A. (2013). Temporal variability of thermal refuges and water temperature patterns in an Atlantic salmon river. *Remote Sensing of Environment*, *136*, 358–373. https://doi.org/10.1016/j.rse.2013.05.018

Dugdale, S. J., Hannah, D. M., & Malcolm, I. A. (2017). River temperature modelling: A review of process-based approaches and future directions. *Earth-Science Reviews*, *175*, 97–113. https://doi.org/10.1016/j.earscirev.2017.10.009

Dugdale, S. J., Hannah, D. M., & Malcolm, I. A. (2020). An evaluation of different forest cover geospatial data for riparian shading and river temperature modelling. *River Research and Applications*, *36*(5), 709–723. https://doi.org/10.1002/rra.3598

Dugdale, S. J., Kelleher, C. A., Malcolm, I. A., Caldwell, S., & Hannah, D. M. (2019). Assessing the potential of drone-based thermal infrared imagery for quantifying river temperature heterogeneity. *Hydrological Processes*, *33*(7), 1152–1163. https://doi.org/10.1002/hyp.13395

Dugdale, S. J., Malcolm, I. A., & Hannah, D. M. (2019). Drone-based structure-from-motion provides accurate forest canopy data to assess shading effects in river temperature models. *Science of the Total Environment*, *678*, 326–340. https://doi.org/10.1016/j.scitotenv.2019.04.229

Dugdale, S. J., Malcolm, I. A., & Hannah, D. M. (2024). Understanding the effects of spatially variable riparian tree planting strategies to target water temperature reductions in rivers. *Journal of Hydrology*, *635*, 131163. https://doi.org/10.1016/j.jhydrol.2024.131163

Gallice, A., Bavay, M., Brauchli, T., Comola, F., Lehning, M., & Huwald, H. (2016). StreamFlow 1.0: An extension to the spatially distributed snow model Alpine3D for hydrological modelling and deterministic stream temperature prediction. *Geoscientific Model Development*, *9*(12), 4491–4519. https://doi.org/10.5194/gmd-9-4491-2016

Garner, G., Malcolm, I. A., Sadler, J. P., & Hannah, D. M. (2017). The role of riparian vegetation density, channel orientation and water velocity in determining river temperature dynamics. *Journal of Hydrology*, *553*, 471–485. https://doi.org/10.1016/j.jhydrol.2017.03.024

Gatien, P., Arsenault, R., Martel, J.-L., & St-Hilaire, A. (2023). Using the ERA5 and ERA5-Land reanalysis datasets for river water temperature modelling in a data-scarce region. *Canadian Water Resources Journal/Revue Canadienne Des Ressources Hydriques*, *48*(2), 93–110. https://doi.org/10.1080/07011784.2022.2113917

Gerecht, K. E., Cardenas, M. B., Guswa, A. J., Sawyer, A. H., Nowinski, J. D., & Swanson, T. E. (2011). Dynamics of hyporheic flow and heat transport across a bed-to-bank continuum in a large regulated river. *Water Resources Research*, *47*(3). https://doi.org/10.1029/2010WR009794

Gupta, H. V., Kling, H., Yilmaz, K. K., & Martinez, G. F. (2009). Decomposition of the mean squared error and NSE performance criteria: Implications for improving hydrological modelling. *Journal of Hydrology*, *377*(1), 80–91. https://doi.org/10.1016/j.jhydrol.2009.08.003

19447973, 2025, 9, Downloaded from https://agupubs.onlinelibrary.wiley.com/doi/10.1029/2024WR038860 by Schweizerische Akademie Der, Wiley Online Library on [26/09/2025]. See the Terms and Conditions (https://onlinelibrary.wiley.com/terms-and-conditions) on Wiley Online Library for rules of use; OA articles are governed by the applicable Creative Commons License

Hall, A., & Selker, J. S. (2021). High-resolution temperature modeling of stream reconstruction alternatives. *River Research and Applications*, *37*(7), 931–942. https://doi.org/10.1002/rra.3824

Hannah, D. M., Malcolm, I. A., Soulsby, C., & Youngson, A. F. (2004). Heat exchanges and temperatures within a salmon spawning stream in the Cairngorms, Scotland: Seasonal and sub-seasonal dynamics. *River Research and Applications*, *20*(6), 635–652. https://doi.org/10.1002/rra.771

Hannah, D. M., Malcolm, I. A., Soulsby, C., & Youngson, A. F. (2008). A comparison of forest and moorland stream microclimate, heat exchanges and thermal dynamics. *Hydrological Processes*, *22*(7), 919–940. https://doi.org/10.1002/hyp.7003

HEC (Hydrologic Engineering Center). (2022). HEC-RAS River Analysis System, Version 6.3 [Software]. *U.S. Army Corps of Engineers, Institute for Water Resources*. Retrieved from https://www.hec.usace.army.mil/software/hec-ras/download.aspx

Hester, E. T., Doyle, M. W., & Poole, G. C. (2009). The influence of in-stream structures on summer water temperatures via induced hyporheic exchange. *Limnology & Oceanography*, *54*(1), 355–367. https://doi.org/10.4319/lo.2009.54.1.0355

Hofierka, J., & Suri, M. (2002). The solar radiation model for Open source GIS: Implementation and applications. In *Proceedings of the Open Source GIS-GRASS Users Conference* (Vol. 2002, pp. 51–70).

Hrachowitz, M., Fovet, O., Ruiz, L., Euser, T., Gharari, S., Nijzink, R., et al. (2014). Process consistency in models: The importance of system signatures, expert knowledge, and process complexity. *Water Resources Research*, *50*(9), 7445–7469. https://doi.org/10.1002/2014WR015484

Keery, J., Binley, A., Crook, N., & Smith, J. W. N. (2007). Temporal and spatial variability of groundwater–surface water fluxes: Development and application of an analytical method using temperature time series. *Journal of Hydrology*, *336*(1), 1–16. https://doi.org/10.1016/j.jhydrol.2006.12.003

Kirchner, J. W. (2006). Getting the right answers for the right reasons: Linking measurements, analyses, and models to advance the science of hydrology. *Water Resources Research*, *42*(3). https://doi.org/10.1029/2005WR004362

Kurylyk, B. L., Irvine, D. J., Carey, S. K., Briggs, M. A., Werkema, D. D., & Bonham, M. (2017). Heat as a groundwater tracer in shallow and deep heterogeneous media: Analytical solution, spreadsheet tool, and field applications. *Hydrological Processes*, *31*(14), 2648–2661. https://doi.org/10.1002/hyp.11216

Kurylyk, B. L., MacQuarrie, K. T. B., & Voss, C. I. (2014). Climate change impacts on the temperature and magnitude of groundwater discharge from shallow, unconfined aquifers. *Water Resources Research*, *50*(4), 3253–3274. https://doi.org/10.1002/2013WR014588

Leach, J. A., Kelleher, C., Kurylyk, B. L., Moore, R. D., & Neilson, B. T. (2023). A primer on stream temperature processes. *WIREs Water*, *10*(4), e1643. https://doi.org/10.1002/wat2.1643

Leach, J. A., & Moore, R. D. (2010). Above-stream microclimate and stream surface energy exchanges in a wildfire-disturbed riparian zone. *Hydrological Processes*, *24*(17), 2369–2381. https://doi.org/10.1002/hyp.7639

Leach, J. A., & Moore, R. D. (2014). Winter stream temperature in the rain-on-snow zone of the Pacific Northwest: Influences of hillslope runoff and transient snow cover. *Hydrology and Earth System Sciences*, *18*(2), 819–838. https://doi.org/10.5194/hess-18-819-2014

Loicq, P., Moatar, F., Jullian, Y., Dugdale, S. J., & Hannah, D. M. (2018). Improving representation of riparian vegetation shading in a regional stream temperature model using LiDAR data. *Science of the Total Environment*, *624*, 480–490. https://doi.org/10.1016/j.scitotenv.2017.12.129

Maheu, A., & Caissie, D. (2023). Spatial and temporal variability of the solar radiation heat flux in streams of a forested catchment. *Canadian Water Resources Journal/Revue Canadienne Des Ressources Hydriques*, *48*(2), 206–221. https://doi.org/10.1080/07011784.2023.2167609

Maheu, A., Caissie, D., St-Hilaire, A., & El-Jabi, N. (2014). River evaporation and corresponding heat fluxes in forested catchments. *Hydrological Processes*, *28*(23), 5725–5738. https://doi.org/10.1002/hyp.10071

Malcolm, I. A., Hannah, D. M., Donaghy, M. J., Soulsby, C., & Youngson, A. F. (2004). The influence of riparian woodland on the spatial and temporal variability of stream water temperatures in an upland salmon stream. *Hydrology and Earth System Sciences*, *8*(3), 449–459. https://doi.org/10.5194/hess-8-449-2004

Mameri, D., Hayes, D. S., Führer, S., Fauchery, E., Schmutz, S., Monserat, A., et al. (2023). Cold thermopeaking-induced drift of nase Chondrostoma nasus larvae. *Aquatic Sciences*, *85*(2), 56. https://doi.org/10.1007/s00027-023-00955-x

MeteoSwiss. (2025). Automatic weather stations [Dataset]. *Open Data*. Retrieved from https://www.meteoswiss.admin.ch/services-and-publications/service/open-data.html

Michel, A., Schaefli, B., Wever, N., Zekollari, H., Lehning, M., & Huwald, H. (2022). Future water temperature of rivers in Switzerland under climate change investigated with physics-based models. *Hydrology and Earth System Sciences*, *26*(4), 1063–1087. https://doi.org/10.5194/hess-26-1063-2022

Moore, R. D., Sutherland, P., Gomi, T., & Dhakal, A. (2005). Thermal regime of a headwater stream within a clear-cut, coastal British Columbia, Canada. *Hydrological Processes*, *19*(13), 2591–2608. https://doi.org/10.1002/hyp.5733

Nearing, G. S., Kratzert, F., Sampson, A. K., Pelissier, C. S., Klotz, D., Frame, J. M., et al. (2021). What role does hydrological science play in the age of machine learning? *Water Resources Research*, *57*(3), e2020WR028091. https://doi.org/10.1029/2020WR028091

OFEV. (2017a). Eclusées—Mesures d'assainissement, Un module de l'aide à l'exécution Renaturation des eaux. Retrieved from https://www.bafu.admin.ch/bafu/fr/home/themen/thema-wasser/wasser--publikationen/publikationen-wasser/schwall-sunk-massnahmen.html

OFEV. (2017b). Impulsions pour une adaptation de la Suisse aux changements climatiques. Retrieved from https://www.bafu.admin.ch/bafu/fr/home/themen/thema-klima/klima--publikationen-und-studien/publikationen-klima/impulse-fuer-klimaangepasste-schweiz.html

OpenAI. (2024).ChatGPT (GPT-4) [Large language model]. Retrieved from https://chat.openai.com/

O'Sullivan, A. M., Devito, K. J., Ogilvie, J., Linnansaari, T., Pronk, T., Allard, S., & Curry, R. A. (2020). Effects of topographic resolution and geologic setting on spatial statistical river temperature models. *Water Resources Research*, *56*(12), e2020WR028122. https://doi.org/10.1029/2020WR028122

Ouellet, V., St-Hilaire, A., Dugdale, S. J., Hannah, D. M., Krause, S., & Proulx-Ouellet, S. (2020). River temperature research and practice: Recent challenges and emerging opportunities for managing thermal habitat conditions in stream ecosystems. *Science of the Total Environment*, *736*, 139679. https://doi.org/10.1016/j.scitotenv.2020.139679

Poole, G. C., & Berman, C. H. (2001). An ecological perspective on in-stream temperature: Natural heat dynamics and mechanisms of Human-CausedThermal degradation. *Environmental Management*, *27*(6), 787–802. https://doi.org/10.1007/s002670010188

Rahmani, F., Lawson, K., Ouyang, W., Appling, A., Oliver, S., & Shen, C. (2021). Exploring the exceptional performance of a deep learning stream temperature model and the value of streamflow data. *Environmental Research Letters*, *16*(2), 024025. https://doi.org/10.1088/1748-9326/abd501

Ritter, A., & Muñoz-Carpena, R. (2013). Performance evaluation of hydrological models: Statistical significance for reducing subjectivity in goodness-of-fit assessments. *Journal of Hydrology*, *480*, 33–45. https://doi.org/10.1016/j.jhydrol.2012.12.004

Sawyer, A. H., Bayani Cardenas, M., Bomar, A., & Mackey, M. (2009). Impact of dam operations on hyporheic exchange in the riparian zone of a regulated river. *Hydrological Processes*, *23*(15), 2129–2137. https://doi.org/10.1002/hyp.7324

Sinokrot, B. A., & Stefan, H. G. (1993). Stream temperature dynamics: Measurements and modeling. *Water Resources Research*, *29*(7), 2299–2312. https://doi.org/10.1029/93WR00540

19447973, 2025, 9, Downloaded from https://agupubs.onlinelibrary.wiley.com/doi/10.1029/2024WR038860 by Schweizerische Akademie Der, Wiley Online Library on [26/09/2025]. See the Terms and Conditions (https://onlinelibrary.wiley.com/terms-and-conditions) on Wiley Online Library for rules of use; OA articles are governed by the applicable Creative Commons License

Stadnyk, T. A., & Holmes, T. L. (2023). Large scale hydrologic and tracer aided modelling: A review. *Journal of Hydrology*, *618*, 129177. https://doi.org/10.1016/j.jhydrol.2023.129177

St-Hilaire, A., Morin, G., El-Jabi, N., & Caissie, D. (2000). Water temperature modelling in a small forested stream: Implication of forest canopy and soil temperature. *Canadian Journal of Civil Engineering*, *27*(6), 1095–1108. https://doi.org/10.1139/l00-021

Sun, J., Di Nunno, F., Sojka, M., Ptak, M., Luo, Y., Xu, R., et al. (2024). Prediction of daily river water temperatures using an optimized model based on NARX networks. *Ecological Indicators*, *161*, 111978. https://doi.org/10.1016/j.ecolind.2024.111978

Swissrivers. (2025). Hydrological data portal—Canton of Fribourg [Dataset]. Retrieved from https://fribourg.swissrivers.ch

Thierrin, J. (1990). Contribution à l'étude des eaux souterraines de la région de Fribourg (Suisse occidentale).

Todorović, A., Grabs, T., & Teutschbein, C. (2022). Advancing traditional strategies for testing hydrological model fitness in a changing climate. *Hydrological Sciences Journal*, *67*(12), 1790–1811. https://doi.org/10.1080/02626667.2022.2104646

Toffolon, M., & Piccolroaz, S. (2015). A hybrid model for river water temperature as a function of air temperature and discharge. *Environmental Research Letters*, *10*(11), 114011. https://doi.org/10.1088/1748-9326/10/11/114011

Topp, S. N., Barclay, J., Diaz, J., Sun, A. Y., Jia, X., Lu, D., et al. (2023). Stream temperature prediction in a shifting environment: Explaining the influence of deep learning architecture. *Water Resources Research*, *59*(4), e2022WR033880. https://doi.org/10.1029/2022WR033880

Trimmel, H., Weihs, P., Leidinger, D., Formayer, H., Kalny, G., & Melcher, A. (2018). Can riparian vegetation shade mitigate the expected rise in stream temperatures due to climate change during heat waves in a human-impacted pre-alpine river? *Hydrology and Earth System Sciences*, *22*(1), 437–461. https://doi.org/10.5194/hess-22-437-2018

van Vliet, M. T. H., Franssen, W. H. P., Yearsley, J. R., Ludwig, F., Haddeland, I., Lettenmaier, D. P., & Kabat, P. (2013). Global river discharge and water temperature under climate change. *Global Environmental Change*, *23*(2), 450–464. https://doi.org/10.1016/j.gloenvcha.2012.11.002

Vanzo, D., Siviglia, A., Carolli, M., & Zolezzi, G. (2016). Characterization of sub-daily thermal regime in alpine rivers: Quantification of alterations induced by hydropeaking. *Hydrological Processes*, *30*(7), 1052–1070. https://doi.org/10.1002/hyp.10682

Wade, J., Kelleher, C., & Kurylyk, B. L. (2024). Incorporating physically-based water temperature predictions into the National water model framework. *Environmental Modelling & Software*, *171*, 105866. https://doi.org/10.1016/j.envsoft.2023.105866

Wanders, N., van Vliet, M. T. H., Wada, Y., Bierkens, M. F. P., & van Beek, L. P. H. (2019). High-resolution global water temperature modeling. *Water Resources Research*, *55*(4), 2760–2778. https://doi.org/10.1029/2018WR023250

Wawrzyniak, V., Allemand, P., Bailly, S., Lejot, J., & Piégay, H. (2017). Coupling LiDAR and thermal imagery to model the effects of riparian vegetation shade and groundwater inputs on summer river temperature. *Science of the Total Environment*, *592*, 616–626. https://doi.org/10.1016/j.scitotenv.2017.03.019

Webb, B. W., & Zhang, Y. (1997). Spatial and seasonal variability in the components of the river heat budget. *Hydrological Processes*, *11*(1), 79–101. https://doi.org/10.1002/(SICI)1099-1085(199701)11:1<79::AID-HYP404>3.0.CO;2-N

Woltemade, C. J., & Hawkins, T. W. (2016). Stream temperature impacts because of changes in air temperature, land cover and stream discharge: Navarro River Watershed, California, USA. *River Research and Applications*, *32*(10), 2020–2031. https://doi.org/10.1002/rra.3043

Zhang, Z., & Johnson, B. E. (2016). *Aquatic nutrient simulation modules (NSMs) developed for hydrologic and hydraulic models*. US Army Engineer Research and Development Center, Environmental Laboratory.

Zhu, S., & Piotrowski, A. P. (2020). River/stream water temperature forecasting using artificial intelligence models: A systematic review. *Acta Geophysica*, *68*(5), 1433–1442. https://doi.org/10.1007/s11600-020-00480-7

Zolezzi, G., Siviglia, A., Toffolon, M., & Maiolini, B. (2011). Thermopeaking in Alpine streams: Event characterization and time scales. *Ecohydrology*, *4*(4), 564–576. https://doi.org/10.1002/eco.132

References From the Supporting Information

Toffolon, M., Siviglia, A., & Zolezzi, G. (2010). Thermal wave dynamics in rivers affected by hydropeaking. *Water Resources Research*, *46*(8). https://doi.org/10.1029/2009WR008234

19447973, 2025, 9, Downloaded from https://agupubs.onlinelibrary.wiley.com/doi/10.1029/2024WR038860 by Schweizerische Akademie Der, Wiley Online Library on [26/09/2025]. See the Terms and Conditions (https://onlinelibrary.wiley.com/terms-and-conditions) on Wiley Online Library for rules of use; OA articles are governed by the applicable Creative Commons License